aerospace

MDPI

Article

Impact of Alternative Propulsion Systems on Contrail Formation and Lifetime

Judith Rosenow *, Thomas F. Geyer and Lars Enghardt

Environmental Impact and Sensor Technology Department, DLR German Aerospace Center, 03046 Cottbus, Germany; thomas.geyer@dlr.de (T.F.G.); lars.enghardt@dlr.de (L.E.)
* Correspondence: judith.rosenow@dlr.de

Abstract

The reduction in aviation-induced climate impacts requires not only decreasing CO_2 emissions, but also mitigating non-CO_2 effects such as persistent contrail cirrus. Alternative propulsion systems and fuels are therefore discussed as potential pathways toward climate-neutral aviation. However, their influence on contrail formation and evolution remains insufficiently understood, particularly regarding how emission characteristics translate into contrail microphysical behavior and lifetime. This study aims to bridge this knowledge gap by systematically evaluating the contrail-forming potential of Sustainable Aviation Fuel (SAF) and hydrogen-based propulsion systems, with a clear focus on identifying the key emission parameters that govern contrail persistence. To assess the impact of reduced particle emissions on contrail evolution, scenarios with lower initial ice crystal number concentrations N_{ice}, representative of alternative propulsion concepts, were simulated using a Gaussian plume contrail evolution model. The results demonstrate that high ice crystal number concentrations ($N_{ice} \approx 10^{14}$–$10^{15}\,kg^{-1}$), characteristic of kerosene and many SAF combustion cases, lead to persistent contrails with lifetimes of approximately 9–12 h due to suppressed crystal growth and sedimentation. Conversely, low initial ice crystal concentrations ($N_{ice} \approx 10^{9}$–$10^{10}\,kg^{-1}$), expected for hydrogen systems under aerosol-limited nucleation conditions, promote short-lived contrails in the order of minutes. The findings indicate that contrail impacts are influenced not only by the fuel type itself, but also by combustion processes, atmospheric conditions, and the prevailing nucleation mechanisms. Consequently, the potential of SAF and hydrogen propulsion systems to mitigate contrail-related climate effects will likely depend on further technological optimization as well as additional experimental and in-flight observations to better quantify their atmospheric impacts. This work underscores the importance of linking emission measurements directly to contrail microphysics and provides a framework for evaluating future propulsion technologies based on their actual contrail-forming potential, rather than solely on fuel composition or CO_2 reduction.

Keywords: sustainableaviation fuels; hydrogenaviation; contrailformation; ice-nucleating particles; non-CO_2climate effects

Check for updates

Academic Editor: Miroslav Kelemen

Received: 30 June 2026
Revised: 12 August 2026
Accepted: 13 August 2026
Published: 14 August 2026

Correction Statement: This article has been republished with a minor change. The change does not affect the scientific content of the article and further details are available within the backmatter of the website version of this article.

Copyright: © 2026 by the authors. Licensee MDPI, Basel, Switzerland. This article is an open access article distributed under the terms and conditions of the Creative Commons Attribution (CC BY) license.

1. Introduction

Contrails form in sufficiently cold and humid regions of the upper troposphere (typically 8–13 km altitude) as line-shaped ice clouds induced by aircraft exhaust emissions [1,2]. According to the World Meteorological Organization (WMO), contrails are defined as artificial ice clouds generated by jet aircraft cruising in the upper troposphere, with persistent

contrails being those that remain visible for at least 10 min, classified by the WMO as Cirrus homogenitus [3]. These persistent contrails represent the only man-made type of ice clouds and are the primary source of aviation-induced non-CO_2 climate impacts. In this study, it is distinguished between short-lived contrails (those dissipating within less than 10 min) and persistent contrails, which are the focus of our analysis due to their significant radiative effects. While the term contrail cirrus is sometimes used to describe the diffuse, widespread cirrus-like structures that evolve from persistent contrails, a morphological distinction is not made in this work, as the focus lies on the initial formation and lifetime dynamics rather than the subsequent evolution into large-scale cirrus fields. Instead, the broader term Aircraft-Induced Cloudiness (AIC) is used to refer to the collective phenomenon of contrails and their long-lived remnants, in line with the definition provided by Kärcher [3]. These clouds perturb the Earth's radiation balance by enhancing the greenhouse effect through longwave radiation trapping, while having a minor cooling effect via increased albedo. In some atmospheric conditions, the resulting radiative forcing from contrails and their persistent remnants exceeds that of aviation CO_2 emissions alone [2,4], making them a critical target for climate mitigation strategies in aviation.

While operational mitigation strategies such as flight altitude adjustments, routing to avoid ice-supersaturated regions, or contrail avoidance forecasting have been proposed [5,6], their implementation is subject to significant operational, economic, and regulatory constraints. In particular, such measures may lead to trade-offs with increased fuel burn, airspace complexity, or limited global applicability, thereby restricting their long-term mitigation potential [6,7].

Moreover, contrails represent only one component of aviation's climate impact, which also includes CO_2, NO_x, water vapor, and aerosol emissions. Consequently, a comprehensive decarbonization strategy requires a system-level perspective that addresses multiple emission pathways simultaneously. In this context, alternative propulsion and fuel systems, such as hydrogen-based combustion or fuel cell technologies, as well as SAFs are of particular interest, as they could fundamentally alter the emission characteristics of aircraft engines [8].

The choice of fuel and propulsion concept directly influences the type, number, and physicochemical properties of emitted particles, especially soot and volatile aerosols, which act as condensation nuclei for ice formation [3]. These changes, in turn, affect contrail formation thresholds, ice crystal number concentrations, and the radiative properties of contrail cirrus. Therefore, investigating alternative propulsion systems is essential not only for reducing CO_2 emissions but also for understanding and potentially mitigating non-CO_2 climate effects at their physical origin, rather than relying solely on operational avoidance strategies.

Alternative propulsion concepts and fuel types have therefore attracted increasing scientific and regulatory attention. Hydrogen, either combusted in gas turbines or utilized in fuel cell systems, eliminates direct CO_2 emissions. However, its implications for contrail formation and properties remain insufficiently understood, particularly due to the increased water vapor emissions associated with hydrogen combustion, up to 2.5 times higher than those from conventional kerosene per unit of energy [9]. This substantial increase in water vapor input significantly alters the thermodynamic conditions in the upper troposphere and may promote homogeneous nucleation, potentially leading to higher initial ice crystal number concentrations and influencing contrail persistence. As such, the climatic impact of hydrogen-based propulsion cannot be assessed solely based on CO_2 reduction; the enhanced water vapor emissions must be explicitly considered in future climate assessments to accurately evaluate the net effect on contrail formation, cirrus evolution, and overall aviation-induced radiative forcing. SAFs, characterized by diverse chemical compositions,

have been investigated in numerous ground-based and in-flight measurement campaigns. Although SAFs generally lead to reduced soot particle emissions compared to conventional kerosene, experimental observations indicate substantial variability, and their effect on contrail ice crystal number concentrations has not yet been consistently established.

This study addresses open questions regarding the influence of hydrogen and SAF combustion on contrail microphysics. Specifically, it tests the hypotheses that (i) hydrogen combustion does not produce effective condensation nuclei, (ii) SAFs lead to reduced soot particle emissions relative to kerosene, and (iii) contrails formed from hydrogen combustion contain significantly fewer ice crystals than those formed from SAFs. By integrating theoretical analysis, emission characterization, and life-cycle modeling approaches, this work aims to provide a comprehensive assessment of the potential of alternative aviation technologies to mitigate contrail-related climate impacts.

This paper is structured as follows. After the introduction and a review of the state of the art, alternative aviation propulsion and fuel concepts are presented in Section 2. Section 3 introduces the fundamentals of contrail formation and ice nucleation, examines the role of emissions in contrail development, and analyzes the relationship between particle emissions, initial ice crystal numbers, and contrail persistence. Finally, the paper concludes with a summary of the main findings and provides an outlook on future research needs in Section 4.

1.1. State of the Art

The formation and climate impact of aircraft contrails have been extensively studied over the past decades, with a particular focus on their microphysical properties and radiative effects. Contrail formation is primarily governed by ambient thermodynamic conditions and the properties of aircraft exhaust emissions, especially the number and composition of aerosol particles that act as ice nucleation sites [1,3]. Among these, soot particles emitted during hydrocarbon fuel combustion play a dominant role as condensation nuclei, directly influencing the initial ice crystal number concentration and subsequent contrail evolution [3,10].

Beside soot particles, atmospheric particulates that serve as sites for water vapor condensation, initiate cloud droplet formation. A wide range of naturally occurring aerosols act as Cloud COndensation Nuclei (CCN), each with distinct hygroscopic properties that influence their effectiveness. Among the most important natural CCN are:

- Sea salt aerosols: Generated by ocean wave spray, these particles are highly hygroscopic and efficient CCN, particularly over marine regions [11,12]. They are a dominant source of CCN in coastal and open-ocean environments.
- Sulfate aerosols: Formed through the oxidation of sulfur dioxide (SO_2) from volcanic emissions or biogenic dimethyl sulfide (DMS) released by phytoplankton [13,14]. Sulfate particles are highly hygroscopic and play a key role in marine cloud formation, especially in remote oceanic areas [15,16].
- Phytoplankton-derived dimethyl sulfide (DMS): Marine phytoplankton produce DMS, which is oxidized in the atmosphere to form sulfuric acid and subsequently sulfate aerosols [12,13]. This process is central to the CLAW hypothesis, which proposes a climate-regulating feedback loop between oceanic productivity, cloud albedo, and global temperature [13].
- Mineral dust and clay particles: Emitted from arid regions via wind erosion, these particles are less hygroscopic than sea salt or sulfate but can still act as CCN under certain conditions [11]. They are particularly important in continental and desert regions.
- Secondary organic aerosols (SOA): Formed from the atmospheric oxidation of volatile organic compounds (VOCs) emitted by vegetation and other natural sources [11].

While generally less hygroscopic than sulfate or sea salt, SOA can contribute to CCN populations, especially in forested regions.

It is important to note that many of these particles are not pure but exist as complex mixtures (e.g., sulfate mixed with organic carbon), which can significantly alter their hygroscopicity and CCN activity [11]. In contrast, soot and black carbon particles—though effective ice nuclei in colder regions—are generally poor CCN due to their hydrophobic nature [11]. Similarly, mineral dust and organic carbon particles exhibit low hygroscopicity and are less effective as CCN compared to sea salt and sulfate.

The abundance and composition of CCN directly influence cloud microphysics, including droplet number concentration, cloud lifetime, albedo, and precipitation efficiency [15]. These effects, in turn, play a critical role in Earth's radiative balance and climate system [17]. For example, the CLAW hypothesis suggests that warming oceans may enhance phytoplankton blooms, increasing DMS emissions and thus cloud albedo, potentially creating a negative feedback loop that mitigates warming [13]. Conversely, the anti-CLAW hypothesis proposes that ocean stratification reduces nutrient availability, suppressing phytoplankton and reducing CCN, leading to a positive feedback that amplifies warming [18].

Furthermore, volcanic eruptions inject large quantities of SO_2 into the atmosphere, which is rapidly oxidized to form sulfate aerosols that act as CCN and contribute to global cooling by enhancing cloud albedo [14,19]. This process underscores the significant role of natural sources in modulating atmospheric aerosol concentrations and climate.

A substantial body of work has demonstrated that reducing soot emissions can significantly alter contrail properties. Numerical studies by [3,10,20] show that lower soot particle number concentrations lead to fewer initial ice crystals, which may result in optically thinner contrails with modified lifetimes and radiative forcing. These findings are supported by experimental evidence from flight campaigns such as ACCESS [21] and Emission and Climate Impact of Alternative Fuels (ECLIF) [22], where alternative fuels were tested under real flight conditions.

SAFs, particularly those with low aromatic content, have been shown to reduce soot emissions compared to conventional Jet A-1 fuel. In situ measurements during the ECLIF [22] and ECLIF2/ND-MAX campaigns [22] demonstrated reductions in non-volatile particulate matter by up to 50–70%, depending on the fuel blend and engine operating conditions [23,24]. This reduction in soot emissions has been linked to a decrease in contrail ice crystal number concentrations. However, the relationship is not strictly linear and exhibits significant variability due to atmospheric conditions and plume processing [24]. Consequently, while SAFs are generally associated with a mitigation potential for contrail climate effects, uncertainties remain regarding the contrail lifetime, magnitude, and robustness of this effect.

Recent experimental studies have demonstrated that SAFs with aromatic hydrocarbon content below 8% exhibit significantly reduced soot emissions compared to conventional jet fuel [25]. This threshold is critical because aromatic compounds are the primary precursors to soot formation during combustion. When aromatic content is reduced below 8%, the combustion process shifts toward more complete oxidation, leading to a substantial decrease in the formation of Polycyclic aromatic hydrocarbon (PAH)s and, consequently, soot particle number concentrations [26]. Ref. [24] reported that SAF blends with aromatic content below 8% achieved soot emission reductions of up to 90% relative to conventional kerosene.

While low-aromatic SAF have been shown to significantly reduce soot and ice number concentrations in contrails—leading to up to 70% reductions in contrail cloudiness under laboratory conditions [24], the aromatic content of most commercially available SAF blends remains substantially higher. For instance, the SAF blends tested in the ECLIF2/ND-MAX campaign, such as SAF1 (51% Ref3 + 49% HEFA-SPK), SAF2 (70% Ref4 + 30% HEFA-SPK)

and SSF1 (59% Ref1 + 41% FT-SPK), had aromatic contents of 8.5% and 9.5%, respectively. In contrast, conventional Jet A-1 fuels (e.g., Ref1–Ref4 in [24]) exhibit aromatic contents of 16.5% to 18.8% [24].

In contrast, hydrogen combustion represents a fundamentally different emission regime. Hydrogen-fueled engines produce no CO_2 and are expected to emit negligible amounts of soot particles, thereby potentially eliminating one of the primary sources of ice nucleation in contrail formation [27,28]. However, hydrogen combustion results in increased water vapor emissions per unit of energy by around 300%, which may enhance contrail formation frequency under suitable atmospheric conditions. Modeling studies conducted by the Aerospace Research Center (DLR) and others suggest that hydrogen-powered aircraft could produce contrails with significantly lower ice crystal number concentrations, but potentially higher ice water content, leading to complex and not yet fully understood climate change effects [7,29].

A recent study based on in-flight measurements (DLR–Airbus–CFM, NEOFUELS/VOLCAN campaign) shows that contrail ice crystal formation at very low soot emission levels remains high, indicating that soot is not the sole controlling factor for ice nucleating particles. Instead, volatile organic compounds and lubricating oil-derived particles become dominant contributors in the low-soot regime [30]. These findings challenge previous assumptions that cleaner combustion and low-sulfur fuels or SAF would proportionally reduce contrail formation, as the measured number of ice crystals remained comparable to conventional kerosene operation despite substantially reduced soot emissions, suggesting no significant decrease in effective ice-nucleating particle formation behind SAF-like conditions [30].

Despite these advances, a direct experimental characterization of contrails formed from hydrogen combustion is currently lacking, and most insights are derived from theoretical considerations and numerical simulations. Furthermore, the interaction between fuel composition, emission characteristics, contrail microphysics, contrail lifetime, and large-scale climate impact remains insufficiently quantified. In particular, comparative studies assessing hydrogen and SAF-based propulsion systems within a consistent framework are scarce. There is a clear need for integrated approaches that combine emission measurements, microphysical modeling, and life cycle assessment to evaluate the full climate impact of alternative aviation technologies. Such approaches are essential to move beyond isolated mitigation strategies and toward a system-level understanding of how propulsion and fuel choices influence both CO_2 and non-CO_2 climate effects.

1.2. Alternative Propulsion and Fuel Concepts

In addition to operational mitigation strategies, such as contrail avoidance routing or adaptive flight altitude optimization, increasing attention has been directed toward alternative propulsion and fuel concepts that fundamentally modify the composition of aircraft exhaust emissions. Since contrail formation strongly depends on emitted water vapor, soot particles, sulfur species, and other aerosol precursors, propulsion technologies based on SAFs or hydrogen may substantially alter contrail microphysics and the resulting non-CO_2 climate effects. Consequently, the following section focuses on the emission characteristics and technological maturity of alternative aviation propulsion pathways relevant to contrail formation.

SAFs are defined by the International Civil Aviation Organization (ICAO) as aviation fuels derived from renewable resources or waste materials that comply with specific sustainability criteria [31]. These criteria are regulated internationally through the Carbon Offsetting and Reduction Scheme for International Aviation (CORSIA) framework and, within the European Union, by the Renewable Energy Directive (RED II) [32]. A

fuel is considered a drop-in fuel if it can be utilized within existing aircraft, engine, and airport fuel infrastructure without requiring hardware modifications while simultaneously fulfilling the physicochemical requirements of conventional Jet A-1 fuel. Fuel quality requirements are specified in ASTM D1655, whereas the ASTM D4054 qualification process evaluates the equivalence of novel SAF pathways. Once approved, production pathways are incorporated into ASTM D7566 and certified for use in commercial aviation [33].

Currently, eight SAF production pathways are approved under ASTM D7566 [31,34]. In addition, three co-processing approaches, in which fossil and biogenic feedstocks are refined simultaneously, are listed under ASTM D1655 [35]. However, due to unresolved sustainability concerns and limited experimental evidence regarding their emission characteristics and life-cycle impact [36,37], co-processing pathways are not considered in this study.

Most certified SAFs are produced from renewable carbonaceous feedstocks such as vegetable oils, waste lipids, animal fats, lignocellulosic biomass, municipal solid waste, or agricultural residues [38–40]. Depending on the pathway, fossil-derived intermediates or external hydrogen sources may still be required during transitional production phases, particularly for Fischer-Tropsch Synthetic Paraffinic Kerosene (FT-SPK), Alcohol-To-Jet (ATJ-SPK), Hydroprocessed Esters and Fatty Acids-Synthetic Paraffinic Kerosene (HEFA-SPK), and Power-to-Liquid (PtL) fuels [41]. Note: E-kerosene is a synthetic aviation fuel produced via PtL) technology, using renewable electricity, water, and captured CO_2. After feedstock pre-treatment, the materials are converted into synthetic kerosene through certified ASTM D7566 conversion pathways involving processes such as gasification, hydroprocessing, alcohol conversion, or Fischer–Tropsch synthesis [42].

The first certified pathway was FT-SPK, approved for blending ratios (i.e., mixing with conventional Jet A-1 and Jet A) up to 50%. In this process, biomass is gasified to produce synthesis gas, which is subsequently converted into hydrocarbons via Fischer-Tropsch synthesis and downstream refining processes [42]. Another major pathway is HEFA-SPK, which utilizes lipid-rich feedstocks such as waste oils or fats that are processed through hydrotreating and isomerization [40]. Additional approved pathways include HFS-SIP, FT-SPK/A, ATJ-SPK, CHJ, HC-HEFA-SPK, and ATJ-SPK/A, each associated with pathway-specific blending limitations and compositional constraints [39].

Beyond biomass-derived fuels, synthetic electrofuels produced via PtL processes are increasingly considered promising long-term decarbonization options. In PtL pathways, renewable electricity is used to electrolytically generate hydrogen from water, which is subsequently combined with captured CO_2 through Fischer-Tropsch synthesis to produce synthetic kerosene. Depending on the process configuration, the required carbon dioxide may originate from industrial point sources or Direct Air Capture systems [39]. Due to their near-aromatic-free composition and low sulfur content, PtL fuels are expected to significantly reduce soot particle emissions compared to fossil kerosene, thereby potentially affecting contrail ice crystal number concentrations.

In parallel to alternative liquid fuels, hydrogen-based propulsion concepts are being actively investigated. Hydrogen may either be combusted directly in modified gas turbines or converted electrochemically within fuel cell systems. Hydrogen combustion engines retain many characteristics of conventional gas turbine architectures, although substantial modifications to combustor geometry and fuel injection systems are required due to hydrogen's high flame speed, low ignition energy, and wide flammability range. While hydrogen combustion can significantly reduce soot emissions and eliminate direct CO_2 emissions, challenges remain regarding combustion stability, flashback prevention, and cryogenic fuel storage [43]. In particular, liquid hydrogen (LH_2) in the tanks exhibits a substantially lower

volumetric energy density than kerosene, necessitating large insulated cryogenic storage tanks and dedicated airport infrastructure [44,45].

Hydrogen fuel cell systems constitute an alternative propulsion architecture in which electricity is generated through the electrochemical reaction between hydrogen and oxygen, producing water vapor as the only reaction product. Such systems are characterized by high efficiency, low acoustic emissions, and the absence of combustion-related soot particles [9,46]. However, considerable challenges remain regarding hydrogen production scalability, storage, distribution infrastructure, thermal management, and aircraft system integration.

To assess the technological maturity of these propulsion pathways, the Commercial Aviation Alternative Fuels Initiative (CAAFI) introduced the Fuel Readyness Level (FRL) concept as a complement to the Technical Readyness Level (TRL) framework [47]. While TRL focuses primarily on technological development and demonstration, FRL additionally captures certification, industrial scalability, and commercial deployment aspects. Since both maturity scales evolve partially independently, simultaneous consideration of TRL and FRL is necessary when evaluating future aviation fuel pathways [47].

Among currently certified SAF pathways, HEFA-SPK and FT-SPK represent the most technologically mature options. Fossil-based FT synthesis has already achieved full commercial deployment (TRL/FRL 9), while biogenic FT pathways remain somewhat less mature [47]. HEFA-SPK, certified in 2011, currently represents the dominant commercial SAF option with both TRL and FRL assessed at level 9. Other pathways, including HC-HEFA, SIP, ATJ-SPK, and CHJ, remain at intermediate maturity levels between TRL/FRL 5 and 7 [48]. The maturity of PtL fuels strongly depends on the CO_2 source and process integration strategy. PtL pathways utilizing concentrated industrial CO_2 streams are already approaching commercial readiness (TRL/FRL 9), whereas pathways relying on Direct Air Capture remain at earlier development stages (TRL 5–7) due to high energy demands and limited industrial scaling [48]. Table 1 provides an overview of the TRL/FRL and feedstock of currently certified SAF pathways.

Table 1. Maturity levels of selected SAF production pathways.

Pathway	Feedstock	TRL/FRL
HEFA-SPK	Waste oils, fats	9
FT-SPK (fossil-based)	Coal/Natural gas	9
FT-SPK (biogenic)	Biomass	7–8
HC-HEFA	Lipids	5–7
SIP	Sugars	5–7
ATJ-SPK	Alcohols	5–7
CHJ	Hydroprocessed hydrocarbons	5–7
PtL	Industrial CO_2	5–7
PtL	Direct Air Capture (DAC) CO_2	5–7

Hydrogen aviation technologies currently exhibit lower maturity levels. Direct hydrogen combustion in gas turbines is generally assessed at approximately TRL 3–4; hydrogen aircraft TRL is not higher than 2–3, whereas hydrogen fuel cell propulsion has progressed toward TRL 6–7 through successful flight demonstrations, including the Dornier 228 fuel cell-powered test aircraft in 2023 [49]. Furthermore, ongoing development programs by Rolls-Royce and the DLR are investigating the feasibility of operating aero-gas turbines with pure hydrogen combustion under realistic aviation conditions [49].

2. Emissions from Alternative Propulsion Systems

2.1. Emissions from SAF Combustion

According to ASTM certification requirements, SAFs must be functionally equivalent to conventional Jet A-1 fuel in terms of combustion performance, energy content, and safety-relevant fuel properties to qualify as drop-in fuels [50]. As a consequence, the primary combustion products under idealized complete combustion conditions should be comparable to those of fossil kerosene. However, due to differences in molecular composition and hydrogen-to-carbon ratios, variations in emission indices and species concentrations may occur under real engine conditions, depending on equivalence ratio, combustor temperature, and engine operating regime [50,51].

In an idealized stoichiometric combustion scenario with complete oxidation and neglecting atmospheric nitrogen chemistry, the principal products are carbon dioxide CO_2 and water vapor H_2O, which are formed according to the oxidation of carbon and hydrogen (C_nH_m) in the fuel

$$C_nH_m + O_2 \longrightarrow CO_2 + H_2O. \quad (1)$$

In realistic atmospheric combustion environments, however, the presence of nitrogen (N_2) leads to additional formation pathways for nitrogen oxides (NO_x), while trace fuel-bound sulfur (S_x) leads to sulfur oxide (SO_2) emissions. A generalized representation of complete combustion products is then given by:

$$C_nH_mS_x + O_2 + N_2 \longrightarrow CO_2 + H_2O + NO_x + SO_2 + N_2. \quad (2)$$

Carbon dioxide and water vapor represent the dominant products of hydrocarbon combustion and are directly determined by the fuel composition, in particular the hydrogen-to-carbon (H/C) ratio [51]. Since SAFs typically exhibit higher H/C ratios than conventional Jet A-1 fuels, slightly higher water vapor emissions and correspondingly lower specific CO_2 emissions per unit energy can be expected, although these differences remain comparatively small under certification-relevant blending ratios [50].

A key distinction between conventional kerosene and SAFs lies in their possibly reduced content of aromatic and polycyclic aromatic hydrocarbons, as well as their significantly lower sulfur concentrations. These compositional differences strongly influence particulate formation pathways during combustion. In particular, soot formation is driven by aromatic ring growth and PAH chemistry, including Hydrogen Abstraction-aCetylene Addition (HACA) mechanisms that govern soot inception and surface growth processes [52]. The reduced availability of aromatic precursors in SAFs, therefore, should lead to substantially suppressed soot formation rates and lower emissions of non-volatile Particulate Matter (nvPM), which are considered key precursors for contrail ice nucleation [24,53].

In contrast, sulfur oxide (SO_x) emissions are primarily governed by the sulfur content of the fuel and are largely independent of engine operating conditions. While conventional Jet A-1 fuels may contain measurable sulfur fractions, certified SAFs typically exhibit ultra-low sulfur contents below 0.003% [51]. In blended fuels, the resulting sulfur emissions scale proportionally with the fossil fraction of the fuel mixture. Consequently, SAF use leads to a reduction in SO_x emissions relative to conventional aviation fuels, which may further influence aerosol formation processes in the exhaust plume.

In practical aero-engine operation, combustion deviates from the idealized stoichiometric case due to finite mixing rates, local temperature gradients, transient operating conditions, and incomplete oxidation processes. Consequently, aircraft exhaust gases contain a range of intermediate and particulate species in addition to the products of complete combustion. The overall reaction can therefore be approximated as [51]

$$N_2 + O_2 + C_nH_m + S \rightarrow CO_2 + H_2O + N_2 + O_2 + NO_x + CO + UHC + C_{soot} + SO_x. \quad (3)$$

Among the major incomplete combustion products, carbon monoxide (CO) is formed primarily under locally fuel-rich or oxygen-deficient conditions, where the oxidation of carbon to CO_2 remains incomplete [54]. The resulting CO emissions are strongly influenced by combustor architecture, residence time, atomization quality, fuel-air ratio, and engine operating point. Experimental investigations on SAF combustion reveal no universally consistent trend regarding CO emissions. While certain studies report increased CO levels for ATJ-SPK and HEFA-SPK blends [55], others observed reductions relative to conventional kerosene [56]. These discrepancies are mainly attributed to differences in fuel physicochemical properties, including viscosity, volatility, and hydrogen-to-carbon ratio, which affect spray formation and combustion efficiency.

Particulate Matter (PM) emissions from aviation combustion processes comprise both nvPM and volatile Particulate Matter (vPM). The formation of nvPM is primarily associated with incomplete oxidation of hydrocarbon species under high-temperature conditions within the combustor, whereas vPM formation is closely linked to sulfur-containing species and subsequent condensation processes during exhaust cooling [57]. Since particulate emissions are highly relevant for contrail ice nucleation, their reduction constitutes one of the primary motivations for the deployment of alternative aviation fuels.

The dominant component of nvPM is soot (C_{soot}), which forms through pyrolysis and subsequent particle growth mechanisms in fuel-rich combustion zones. These processes involve nucleation, surface growth, agglomeration, and oxidation of carbonaceous particles under elevated temperatures and pressures [57]. In addition to combustion chemistry, soot formation is significantly influenced by combustor geometry, fuel injection strategy, combustor turbulence, and aerodynamic residence time. Due to the substantially lower aromatic and sulfur content of many SAFs, soot precursor formation is suppressed, leading to markedly reduced nvPM emissions compared to conventional Jet A-1 fuel.

Volatile particulate matter originates from gaseous sulfur compounds and semi-volatile hydrocarbons that condense into liquid or solid aerosols as the exhaust plume cools and chemically evolves downstream of the engine exit [57]. Secondary volatile particles may additionally form through atmospheric oxidation reactions involving sulfur oxides and other gaseous exhaust constituents. Since most certified SAFs contain only trace sulfur concentrations, the formation potential of volatile sulfate aerosols is substantially reduced relative to fossil-derived kerosene.

Numerous experimental studies have demonstrated considerable reductions in particulate emissions for different SAF pathways. Reductions in total PM emissions ranging from approximately 7–97% relative to conventional kerosene have been reported for fuels such as FT-SPK, ATJ-SPK, and CH-SKA [56]. In particular, tests with 100% FT-SPK and 50% ATJ-SPK showed reductions of up to 52% and 97%, respectively [58,59]. Similarly, combustion of 100% CH-SKA resulted in moderate reductions of approximately 7–25% across different engine load conditions, while blends containing 50% HEFA-SPK and pure FT-SPK achieved reductions in the order of 40–95% [60]. Overall, the consistently lower aromatic and sulfur fractions of SAFs are widely recognized as the primary drivers for reduced particulate emissions.

Unburned Hydrocarbons (UHC) arise from incomplete fuel oxidation caused by poor atomization, flame quenching, insufficient residence times, or unfavorable local combustion temperatures and pressures, especially in cruise flight at high altitudes. In general, SAF blends tend to reduce UHC emissions due to their lower aromatic content and cleaner

combustion behavior. Nevertheless, elevated UHC levels may still occur when specific fuel properties are not optimally matched to existing combustor designs [55].

Nitrogen oxides (NO_x) are generated predominantly through thermal formation pathways, particularly the Zeldovich mechanism [61], under high-temperature combustion conditions. Unlike soot or sulfur-related species, NO_x formation is influenced primarily by flame temperature, local stoichiometry, residence time, and engine thrust setting rather than by fuel composition itself [62]. Consequently, most experimental studies report only minor or statistically insignificant differences in NO_x emissions between SAFs and conventional kerosene, while observing the expected increase in NO_x production with rising engine power settings.

2.2. Soot Formation Mechanisms in Hydrocarbon Combustion

PAHs play a fundamental role in soot formation during hydrocarbon combustion because they represent the transition between gas-phase fuel decomposition chemistry and the inception of solid carbonaceous particles [63]. In aviation gas turbines, soot formation originates from a sequence of thermochemical reactions occurring under fuel-rich and high-temperature conditions within the combustor [64]. Initially, hydrocarbon fuel molecules undergo thermal cracking and radical-driven oxidation processes, producing smaller unsaturated hydrocarbons such as acetylene (C_2H_2), propargyl radicals (C_3H_3), and benzene (C_6H_6). These intermediate species initiate the formation of aromatic ring structures, which constitute the first step toward PAH growth. Once benzene has formed, it acts as a molecular precursor for subsequent aromatic ring expansion through radical addition and recombination reactions [64].

The HACA pathway (Figure 1) is a well-established mechanism for soot growth, involving the abstraction of hydrogen atoms from aromatic structures, which generates reactive radical sites that undergo addition reactions with acetylene molecules. Repeated cycles of hydrogen abstraction and acetylene addition lead to the progressive formation of increasingly larger PAH, such as naphthalene, phenanthrene, pyrene, and larger fused aromatic ring systems. As molecular size increases, volatility decreases, and intermolecular interactions promote clustering and particle inception.

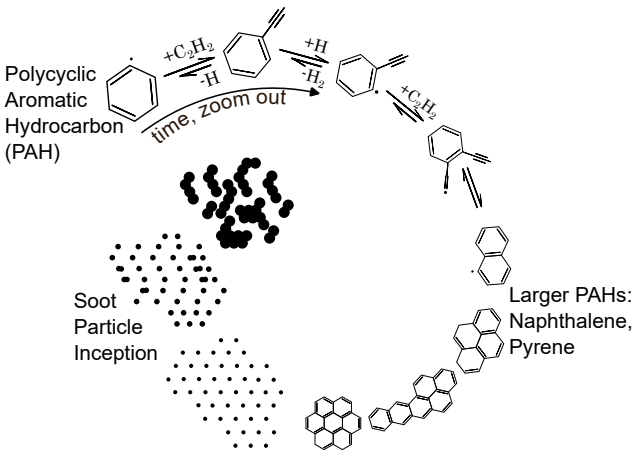

Figure 1. Schematic of soot precursor growth via PAH formation and the HACA mechanism. Fuel pyrolysis produces small unsaturated species (e.g., C_2H_2, C_3H_3, C_6H_6) that form benzene and initiate PAH growth. Increasing size and aromaticity reduce volatility and promote clustering, leading to soot particle inception.

Beyond a critical molecular size, large PAH begin to undergo physical aggregation and chemical clustering processes, forming nano-scale soot precursors. These nascent particles subsequently grow through surface reactions, coagulation, and condensation of

additional hydrocarbon species. Ultimately, this process results in the formation of primary soot particles and larger fractal-like soot aggregates.

The PAH-driven soot formation pathway is widely recognized as the dominant mechanism governing soot production in both laminar and turbulent hydrocarbon flames, including combustion processes in aviation gas turbines [63,64]. Since many SAFs contain substantially lower concentrations of aromatic compounds compared to conventional Jet A-1 fuel, the formation of PAH precursors is suppressed, thereby contributing to the experimentally observed reductions in soot and non-volatile particulate matter emissions.

2.3. Emissions from Hydrogen Combustion

In contrast to hydrocarbon-based aviation fuels, hydrogen does not contain carbon or sulfur. Consequently, combustion of hydrogen does not produce carbon-containing emissions such as CO_2, carbon monoxide (CO), UHC, soot, or sulfur oxides (SO_x) [65]. This represents one of the principal advantages of hydrogen-based propulsion concepts with respect to both climate impact and local air quality. Nevertheless, hydrogen combustion is still associated with the formation of nitrogen oxides (NO_x) due to the high flame temperatures reached during combustion, which thermally activate reactions between atmospheric nitrogen and oxygen.

The overall combustion process can be approximated as

$$O_2 + N_2 + H_2 \rightarrow O_2 + N_2 + H_2O + NO_x. \quad (4)$$

Compared to kerosene combustion, hydrogen combustion produces significantly (i.e., 300%) larger amounts of water vapor per unit of released energy due to the absence of carbon in the fuel and the high hydrogen mass fraction [65]. At the same time, NO_x emissions are generally expected to remain within a similar order of magnitude as modern kerosene combustion systems, since NO_x formation is governed primarily by local flame temperature, residence time, and equivalence ratio rather than fuel composition alone. Advanced combustor concepts, such as lean-premixed hydrogen combustion, are therefore considered essential to limit thermal NO_x formation in future hydrogen aero-engines.

Although soot formation pathways are absent for pure hydrogen combustion, small quantities of particulate matter may still occur. Potential sources include metallic wear particles originating from engine components, lubricant-derived ultrafine particles, or trace impurities within the fuel and combustion system [66]. However, the total PM emissions are expected to be substantially lower than those of conventional hydrocarbon-fueled gas turbines [65]. This reduction is particularly relevant in the context of contrail formation, as soot particles emitted by kerosene combustion currently represent the dominant heterogeneous ice nucleation sites within aircraft exhaust plumes. Despite the increasing scientific interest in hydrogen aviation, direct experimental observations of contrail formation behind hydrogen-powered aircraft engines are not yet available [67].

2.4. Emissions from Aviation Fuel Cell Systems

Hydrogen fuel cell systems differ fundamentally from combustion-based propulsion concepts because energy conversion occurs electrochemically rather than through high-temperature oxidation. Within the fuel cell, hydrogen reacts with oxygen to produce electrical energy, heat, and water vapor according to

$$\frac{1}{2}O_2 + H_2 \rightarrow H_2O. \quad (5)$$

Since fuel cells operate without combustion, neither a flame nor a high-temperature reaction zone is present, effectively eliminating thermal NO_x formation. The electrochemi-

cal conversion of hydrogen produces water vapor as the only direct reaction product [9]. Consequently, hydrogen fuel cell propulsion is considered one of the lowest-emission propulsion concepts currently under investigation for aviation.

Despite the absence of carbon-containing emissions, hydrogen-based propulsion generates substantially more water vapor per unit of released energy than conventional Jet-A1 combustion. While the water vapor emission index for kerosene is approximately 1.23–1.26 kg_{H_2O}/kg_{fuel} [1], hydrogen produces about 2.6 times more water vapor per unit of energy output owing to its fuel chemistry and the complete conversion of hydrogen to water [9,65].

For hydrogen fuel cell propulsion systems, the effective water vapor emissions can become even higher on a mission basis because the electrochemical conversion efficiency reduces waste heat losses while nearly all hydrogen is converted directly into water [9]. In addition, fuel cell aircraft often require lower propulsion efficiency penalties associated with cryogenic storage and balance-of-plant systems, which can alter the total emitted water mass relative to turbofan reference aircraft [9,68]. In addition to increased water emissions, hydrogen propulsion systems release larger fractions of sensible and latent heat into the exhaust plume. Hydrogen combustion exhibits higher specific heat release and flame temperatures than kerosene combustion, resulting in enhanced plume humidity and thermal buoyancy [1,65].

Assuming stoichiometric operation of the fuel cell system, the electrochemical conversion of hydrogen directly determines the reactant and product flow rates. The total current is assumed to be distributed equally among the N fuel cells, resulting in a cell current of $I_{FC} = I/N$. According to Faraday's law, one mole of hydrogen consumed and one mole of water produced each require the transfer of two moles of electrons, whereas one mole of oxygen consumed corresponds to four moles of electrons. Consequently, the molar flow rates are directly proportional to the cell current. The corresponding mass flow rates [g,s^{-1}] are obtained by multiplying the molar flow rates by the respective molar masses, namely $M_{H_2} = 2.01588\ g\,mol^{-1}$, $M_{O_2} = 31.9988\ g\,mol^{-1}$, and $M_{H_2O} = 18.01528\ g\,mol^{-1}$ [69]

$$\dot{M}H_2 = MH_2, N, \frac{I_{FC}}{2F}, \tag{6}$$

$$\dot{M}O_2 = MO_2, N, \frac{I_{FC}}{4F}, \tag{7}$$

$$\dot{M}H_2O = MH_2O, N, \frac{I_{FC}}{2F}, \tag{8}$$

respectively. $F = 96.486\ C\,mol^{-1}$ denotes the Faraday constant. In contrast to hydrocarbon combustion systems, fuel cells convert chemical energy electrochemically rather than through flame-based oxidation. Nevertheless, a significant fraction of the fuel energy is still released as heat due to irreversible electrochemical losses and auxiliary system inefficiencies. The thermal power transferred to the exhaust plume can therefore be approximated by [9]

$$P_{heat} = (1 - \eta_E\,\eta_0)\,\dot{v}_{H_2O}\,\Delta h, \tag{9}$$

where the electric efficiency

$$\eta_E = \frac{U}{\varepsilon} \tag{10}$$

is a function of the ratio of the total fuel cell voltage U [V] and the electromotive force [V]

$$\varepsilon = \frac{\Delta g}{2F}, \tag{11}$$

depending on Gibbs free enthalpy $\Delta g = -228.57\ \mathrm{kJ\,mol^{-1}}$ and Faraday's constant F.

$$\eta_0 = \frac{\Delta g}{\Delta h} \tag{12}$$

is the overall propulsion efficiency, $\Delta h = -241.82\,10^3\ \mathrm{J\,mol^{-1}}$ the molar enthalpy of hydrogen oxidation. Finally, the molar water vapor production rate $\dot{v}_{H_2O}$ [$\mathrm{mol\,s^{-1}}$] can be calculated from

$$\dot{v}_{H_2O} = N\,\frac{I_{\mathrm{FC}}}{2F}. \tag{13}$$

Typical aviation fuel cell systems achieve electrochemical efficiencies of approximately 50–65%, implying that roughly 35–50% of the chemical energy is ultimately dissipated as heat [9,69]. Although this waste-heat fraction is lower than in conventional kerosene combustion engines, where overall propulsion efficiencies are commonly below 40% [51], the lower exhaust temperatures of fuel cell systems fundamentally alter plume thermodynamics and mixing behavior. In contrast to gas turbines, where thermal energy is released predominantly through high-temperature combustion products, fuel cell exhaust plumes are characterized by lower temperatures but substantially higher water vapor concentrations per unit of useful propulsive energy [1,9]. These differences are expected to influence contrail formation processes, plume saturation dynamics, and ice crystal nucleation conditions [70].

3. Fundamentals of Contrail Formation and Ice Nucleation

3.1. Requirements for Contrail Formation

Following the assessment of gaseous and particulate emissions from alternative propulsion and fuel systems, the underlying physical mechanisms governing contrail formation are introduced to establish the connection between exhaust composition and contrail-relevant microphysical processes. Contrails originate from the turbulent mixing of hot, water-vapor-rich aircraft exhaust with the cold and typically low-pressure ambient air of the upper troposphere. During plume dilution, rapid cooling can drive the local thermodynamic state beyond water saturation, thereby initiating condensation and freezing processes. Contrail formation becomes thermodynamically feasible when the Schmidt-Appleman Criterion (SAC) is met, i.e., when the ambient temperature drops below a critical threshold that allows sufficient cooling to compensate for the exhaust heat [1,9]. If the surrounding atmosphere is ice-supersaturated, the newly formed ice crystals may persist and evolve into extended contrail cirrus clouds with substantial radiative forcing potential.

The microphysical evolution of contrails is fundamentally governed by aerosol-mediated nucleation processes. Nucleation denotes the initial phase transition from supersaturated water vapor to liquid droplets or ice particles and may proceed either homogeneously or heterogeneously. Homogeneous freezing occurs spontaneously at temperatures typically below approximately $-38\,^{\circ}\mathrm{C}$ and predominantly involves highly soluble liquid aerosols, such as sulfuric acid-water mixtures [71]. In contrast, heterogeneous nucleation occurs on the surfaces of specialized aerosol particles termed Ice Nucleating Particless (INPs), which substantially reduce the Gibbs free-energy barrier required for ice embryo formation and thereby permit freezing at significantly warmer temperatures [9,72].

Atmospheric INPs originate from both natural and anthropogenic sources, including mineral dust, sea salt, sulfates, soot particles, and metallic aerosols. Their nucleation efficiency depends strongly on particle size, morphology, crystallographic structure, surface roughness, porosity, and chemical composition [72]. Within aviation exhaust plumes, soot particles generated during incomplete hydrocarbon combustion are widely regarded as the dominant anthropogenic INPs governing contrail ice crystal formation [9,73]. These

carbonaceous particles provide highly abundant surfaces for condensation and freezing and are emitted in number concentrations several orders of magnitude larger than most other particulate exhaust species. Their ice nucleation activity is further influenced by nanostructure, surface oxidation state, and chemical aging processes, including coatings by sulfuric acid, ammonia, or organic compounds.

Although metallic and metal-oxide particles originating from engine wear, lubrication systems, or combustion chamber materials may also contribute to heterogeneous ice nucleation, their atmospheric relevance is generally limited by comparatively low emission indices. Typical soot particle emissions from conventional kerosene combustion reach approximately $\sim 10^{15}$ kg^{-1} fuel, whereas metallic particle emissions are commonly restricted to about 10^{7}–10^{8} kg^{-1} fuel [74]. Nevertheless, specific metallic compounds, particularly lead-containing particles, may exhibit exceptionally high intrinsic ice nucleation efficiencies [74]. Under typical cruise conditions, however, background atmospheric INP concentrations are generally insufficient to explain observed contrail ice crystal number densities, implying that aircraft-emitted particles dominate the initiation of contrail formation [73]. Direct observational evidence for the pivotal role of soot particles in contrail formation has been provided by the ECLIF campaign [22]. In-situ vertical plume measurements demonstrated that soot particles are re-released following sublimation of contrail ice crystals, confirming that these particles act as the primary condensation and freezing nuclei within aircraft exhaust plumes [75]. Consequently, any propulsion or fuel technology that significantly alters aerosol emissions, particle composition, or soot number concentrations is expected to substantially influence contrail microphysics, contrail persistence, and ultimately the non-CO_2 climate impact of aviation.

3.2. Ice-Nucleating Particle Emissions from SAF Combustion

As discussed in the previous sections, combustion of SAF derived from carbon-containing feedstocks still produces nvPM, and therefore emits potential condensation and ice-nucleating particles. Nevertheless, numerous experimental studies have demonstrated that SAF combustion generally leads to lower soot particle number emissions (N_{soot}) than conventional Jet A-1 fuel [76]. This reduction is commonly attributed to the lower aromatic content and the higher hydrogen-to-carbon (H/C) ratio in most SAF formulations, which suppress soot precursor formation and inhibit PAH-driven particle growth pathways. As discussed in the State of the Art, recent experimental studies have shown that SAF with aromatic hydrocarbon content below 8% significantly reduce soot emissions compared to conventional jet fuel, due to more complete combustion and lower formation of PAHs. Soot emission reductions of up to 90% have been reported for such fuels [24–26].

However, the experimentally observed reduction in soot emissions shows substantial variability between different measurement campaigns and operating conditions. In particular, aircraft-based measurements systematically report lower N_{soot} values than ground-based engine tests. This discrepancy is likely caused by the inability of stationary test facilities to accurately reproduce representative cruise conditions, including low ambient temperatures, reduced pressure levels, realistic fuel-air ratios, and transient high-altitude combustor operating states. Furthermore, even dedicated flight campaigns remain subject to uncertainty because experimental flight conditions do not fully replicate commercial airline operations under maximum payload and corresponding thrust requirements. The findings from various measurement campaigns are summarized in Figure 2.

Results obtained during the ECLIF III campaign indicate that soot number emissions decrease with increasing combustor inlet temperature T_3 and increasing fuel flow rate for both Jet A-1 and neat HEFA-SPK fuels [76,77]. However, the reduction trend was found to be less pronounced for HEFA-SPK, resulting in a smaller relative decrease in N_{soot} at

elevated combustor temperatures. Similar trends had already been observed during the earlier ECLIF2/ND-MAX campaigns [78]. These findings suggest that combustor operating conditions exert a significant influence on soot formation, potentially comparable to the influence of fuel composition itself.

Interestingly, measurements conducted within the CAAFCER project occasionally reported higher soot number emissions for specific SAF blends compared to neat Jet A-1 fuel. Since the investigated fuels would theoretically be expected to reduce soot formation, these results were attributed primarily to differences in engine operating condition, combustor configuration, engine age, or operational variability rather than intrinsic fuel chemistry [79]. Even within identical engine families, substantial differences in soot emission indices have been reported, highlighting the importance of engine-specific effects.

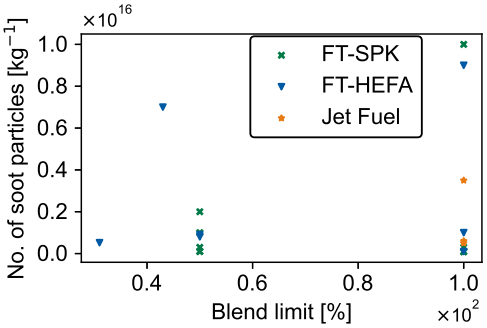

Figure 2. Measured soot particle number emissions N_{soot} from ground-based and in-flight campaigns for various SAF blending ratios [23,52,53,59,76,79–82]. The blend limit refers to the maximum volumetric fraction of SAF that can be blended with conventional jet fuel (Jet A-1) under current certification standards (e.g., ASTM D7566 [34]).

Beyond particle number concentration, the physical properties of soot particles, including particle size distribution, morphology, and effective density, exhibit substantial variability between fuels and operating conditions. For contrail formation and the associated radiative forcing, however, the decisive parameter is ultimately N_{ice}, provided that suitable thermodynamic conditions exist [70]. Since soot particles and other combustion-generated aerosols can act either directly or indirectly as INP, the experimentally observed reductions in particulate emissions from SAF combustion may influence subsequent contrail microphysics.

Several experimental campaigns have therefore investigated particulate matter emissions from alternative fuels in order to estimate their potential impact on contrail formation. Lobo et al. [58] performed ground-based measurements using a CFM56-7B engine operated in an open-air test cell under representative ICAO Landing and Take-Off (LTO) cycle conditions. Measurements with a 50% and a 100% Fischer–Tropsch blend showed total particulate matter reductions of approximately $34 \pm 7\%$ and $52 \pm 7\%$, respectively, with the strongest reduction observed at idle conditions and the weakest reduction at maximum thrust.

Additional measurements were performed during the ECLIF I campaign using an Airbus A320 equipped with V2527-A5 engines [83]. The Semi-Synthetic Jet Fuels (SSJF) (SSJF1: 59% Jet A-1 + 41% SPK; SSJF2: 55% Jet A-1 + 45% SPK) exhibited significantly lower soot emissions. At low engine power (fuel flow < 0.4 kg s^{-1}), SSJF1 reduced soot particle number (PN) emissions by approximately 50-60%, while SSJF2 decreased soot particle mass (PM) emissions by 50-70%. At higher engine power, the reductions remained substantial, with PN emissions decreasing by approximately 30% for SSJF1 and PM emissions by around

20% for SSJF2, demonstrating the soot reduction potential of SPK-blended fuels across the investigated operating conditions.

Many studies distinguish explicitly between vPM and nvPM, thereby enabling a more direct analysis of soot-related emissions. Since soot constitutes the dominant fraction of nvPM in aviation exhaust plumes, nvPM measurements are often used as a surrogate for soot particle emissions. Nevertheless, contributions from other refractory aerosol species cannot be fully excluded, implying that the actual soot fraction may be somewhat lower than the measured total nvPM concentration.

A recent study [30] based on in-flight measurements demonstrated that reducing soot emissions alone, such as through lean-burn combustion or the use of low-sulfur fuels and SAF does not lead to a proportional decrease in ice-nucleating particles relevant for contrail formation. Instead, volatile organic compounds and lubrication oil-derived particles gain relative importance and can sustain high contrail ice crystal numbers even under strongly reduced soot conditions, indicating that SAF-like operating conditions do not automatically lower the overall formation of contrail-relevant particles compared to conventional kerosene [30].

Overall, the currently available experimental evidence consistently indicates that SAF combustion reduces soot particle emissions relative to conventional kerosene combustion. However, despite these reductions, measured soot number emissions generally remain within the order of magnitude range of approximately $10^{14} \leq N_{soot} \leq 10^{15}$ particles per kilogram of fuel, even for high SAF blending ratios or neat SAF operation. Consequently, while SAF combustion clearly alters particulate emission characteristics, the presently available data do not yet provide conclusive evidence that the resulting reduction in soot emissions necessarily translates into proportionally lower contrail ice crystal number concentrations or substantially reduced contrail climate impacts.

3.3. Ice Nucleation Particles from Hydrogen Combustion and Fuel Cell Exhaust

Hydrogen combustion produces exhaust streams dominated by water vapor (which is also a greenhouse gas) and therefore generates substantially higher exhaust humidity than conventional kerosene combustion, while direct emissions of carbon dioxide and soot are largely avoided [66,67]. Nevertheless, elevated combustion temperatures may still promote the formation of NO_x, trace metallic species, and metal oxides, which can potentially act as INP under suitable atmospheric conditions. In addition, Ultrafine Volatile Particle (UFP) originating from lubricating oil vapors, nitrogen-containing compounds, or secondary aerosol formation processes have been identified as possible contributors to particle emissions from hydrogen combustion systems. However, their efficiency as heterogeneous ice nuclei remains insufficiently constrained [66,67].

In contrast, hydrogen fuel cell propulsion systems generate no combustion-related particulate emissions and release primarily water vapor into the atmosphere. Under highly supersaturated conditions, rapid condensation and freezing processes may lead to the formation of large numbers of small ice crystals, resulting in elevated N_{ice} [9]. Since fuel cell systems do not emit soot particles or metallic combustion residues, contrail formation is expected to occur predominantly through homogeneous freezing processes or via activation of pre-existing atmospheric background aerosols [9,67,84,85]. The cruising altitude strongly controls contrail formation because the ambient temperature and the relative humidity with respect to ice (RH_{ice}) determine whether the water vapor released by the engines can nucleate ice crystals. Due to the three times larger H_2O emissions from hydrogen-fueled engines (compared to conventional kerosene-fueled engines), the local saturation ratio behind the exhaust plume is markedly increased. At typical jet-cruising levels (8–12 km) the air is often already close to ice-supersaturation; the extra water vapor pushes the plume into

supersaturation, leading to rapid ice-nucleation and to contrails that are both more frequent and longer-lived than those from conventional aircraft [10,86]. Consequently, even though hydrogen propulsion eliminates CO_2 emissions, its contrail-induced radiative forcing may become a dominant climate impact unless flight altitudes or engine operating conditions are adapted to keep relative humidity over ice below the ice-saturation threshold.

The abundance and physicochemical properties of atmospheric background aerosols exhibit strong regional and temporal variability and include contributions from mineral dust, soot, sulfates, sea salt, and organic particles [67]. Their effectiveness as INP and their influence on contrail microphysics remain associated with considerable uncertainty. Consequently, the frequently stated assumption that hydrogen-powered aircraft emit no relevant INP is only partially valid. While particulate emissions are expected to be substantially reduced compared with kerosene combustion, limited quantities of NO_x-related particles, metallic residues, or UFP may still occur in hydrogen combustion systems, whereas fuel cell-based propulsion is expected to emit almost exclusively water vapor.

The resulting ice particle number concentrations depend nonlinearly on ambient temperature, supersaturation, and background aerosol abundance, with colder atmospheric conditions generally favoring enhanced ice particle formation [84]. Regional aerosol environments further influence the available INP population, with mineral dust particles dominating in arid regions and organic aerosols contributing more strongly in tropical environments [87]. Existing modeling studies therefore predict a broad range of possible ice particle number emissions, typically spanning $N_{INP} = 10^9$–$10^{14}\,m^{-1}$ depending on assumptions regarding water vapor emission indices $E_{I,H2O}$, fuel flow rates, and atmospheric background conditions [67,84,85,87].

3.4. Water Vapor Emission Quantification from SAF Combustion

As discussed in Section 3.3, the formation of ice crystals in exhaust plumes differs fundamentally between SAF, jet A-1 fuel combustion, hydrogen combustion, and hydrogen fuel cell propulsion. In SAF combustion, soot particles constitute the dominant source of INP, whereas hydrogen-based propulsion systems are characterized by substantially increased water vapor emissions and strongly reduced particulate emissions. Consequently, contrail ice formation in hydrogen systems may occur either through homogeneous freezing of emitted water vapor under highly supersaturated conditions or through heterogeneous nucleation involving atmospheric background aerosols. Although soot particles remain the primary driver of ice nucleation in SAF exhaust, the quantification of water vapor emission indices remains relevant for assessing potential impacts on contrail formation, persistence, and optical properties.

Narciso and de Sousa investigated the influence of water vapor emissions from SAF and SAF blends on contrail properties using numerical simulations of contrail microphysics and atmospheric evolution. Their results indicate that enhanced water vapor emissions can promote contrail formation and increase both optical depth and contrail lifetime. The authors further reported that pure SAF fuels may produce substantially higher water vapor emissions than blended fuels, in some cases approaching nearly twice the enhancement observed for lower blending ratios [88].

Experimental measurements obtained during the ECLIF I and ECLIF III flight test campaigns quantified water vapor emission indices for a 41% FT-SPK/Jet A-1 blend and for 100% HEFA-SPK under cruise conditions. Measured values amounted to $E_{I,H2O} = 1.28$ kg/kg for the FT-SPK blend and $E_{I,H2O} = 1.37$ kg/kg for HEFA-SPK. The elevated hydrogen-to-carbon ratio of HEFA-SPK leads to increased water production during combustion and therefore to higher $E_{I,H2O}$ values. Similar values were reported by Narciso and de Sousa, who determined $E_{I,H2O} = 1.295$ kg/kg for a 50% FT-SPK blend and

$E_{I,H2O} = 1.376$ kg/kg for neat HEFA-SPK [88]. Considering differences in blend composition and fuel properties, the experimental and modeled results show good agreement. Since existing studies mainly focus on FT-SPK and HEFA-SPK pathways, the transferability of these findings to other SAF production routes remains uncertain. The currently available results are summarized in Figure 3.

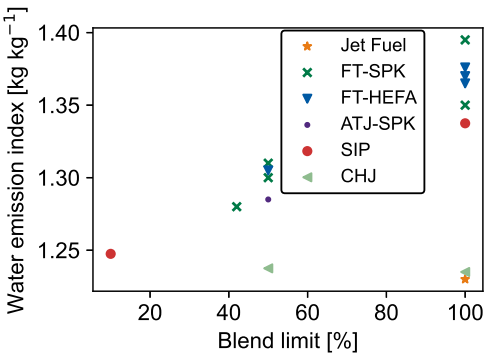

Figure 3. Water vapor emission indices (E_{IH_2O}) for various SAF fuels as a function of blending ratio. Values adapted from [24,52,88].The blend limit refers to the maximum volumetric fraction of SAF that can be blended with conventional jet fuel (Jet A-1) under current certification standards (e.g., ASTM D7566 [34]).

Overall, measured and modeled $E_{I,H2O}$ values for SAF combustion exhibit only moderate variations relative to conventional kerosene fuels and are therefore not expected to substantially modify the availability of INP within SAF exhaust plumes (Figure 3). Nevertheless, the slightly elevated water vapor emissions associated with highly hydrogenated SAF fuels may influence the thermodynamic evolution of the early exhaust plume and potentially affect contrail persistence after the vortex mixing phase, during which ambient supersaturation with respect to ice becomes the dominant controlling factor for contrail lifetime and ice mass development [23].

As mentioned in Section 2.3, direct hydrogen combustion produces significantly larger water vapor emission indices, since water vapor constitutes the primary combustion product. For equal energy release and comparable propulsion efficiency, hydrogen combustion generates approximately 2.6 times more water vapor than kerosene combustion [1], corresponding to typical values of $E_{I,H2O} \approx 9$ kg/kg [9]. Such elevated water vapor emissions may substantially increase the number of formed ice crystals and alter contrail microphysics. However, no in-flight measurements of contrails originating from hydrogen-powered aircraft engines currently exist, and the interaction between emitted water vapor and atmospheric background aerosols remains insufficiently understood. Consequently, large uncertainties persist regarding the resulting ice crystal number concentrations and their influence on contrail optical properties, radiative forcing, and atmospheric lifetime.

Compared with alternative hydrocarbon fuels, both direct hydrogen combustion and hydrogen fuel cell propulsion emit substantially lower quantities of soot and combustion-derived particulate matter. Nevertheless, predicting the resulting ice crystal number concentration remains challenging because contrail formation depends strongly on the dominant nucleation pathway. In heterogeneous nucleation regimes, ice crystal formation is primarily governed by the abundance and physicochemical properties of ambient background aerosols entrained into the exhaust plume. Under homogeneous freezing conditions, however, the influence of background aerosols becomes less significant, since ice crystals form directly from the emitted water vapor under sufficiently cold and supersaturated atmospheric conditions [85].

3.5. Correlation Between Soot Particles and Ice Crystals

The relationship between emitted soot particles (N_{soot}) and apparent ice crystal number (N_{ice}) provides important insight into the initial microphysical properties of contrails, which strongly influence their optical characteristics and atmospheric lifetime. Theoretical studies by Kärcher demonstrated that, in soot-rich exhaust plumes, N_{ice} scales approximately linearly with N_{soot}, whereas ultrafine ambient aerosol particles are expected to contribute only marginally to contrail ice formation [73]. Subsequent investigations further reported a soot activation efficiency of approximately $N_{ice}/N_{soot} = 96\%$ under favorable atmospheric conditions [3]. The following conditions have been investigated as favorable [3]:

- Low temperature: ambient temperatures below $-35°C$ (typical cruising altitudes of 8–12 km) so that water vapor can readily freeze on available nuclei.
- High supersaturation with respect to ice: (i.e., $RH_{ice} > 110\%$) in the wake of the engine, providing enough vapor to grow ice crystals before they evaporate.
- Low background aerosol concentration: background particle number densities $\lesssim 10^2\ cm^{-3}$, ensuring that the soot emitted by the engine dominates the nucleation budget.
- Limited vertical shear: weak mixing that does not dilute the plume and thereby preserves the local supersaturation.

When these conditions are satisfied, soot particles act as the primary ice-nucleating agents.

Figure 4 presents the correlation between N_{soot} and N_{ice} per kilogram of burned fuel measured during ECLIF I (SSF1: 41% FT-SPK), ECLIF II (SAF1: 49% HEFA-SPK, SAF2: 30% HEFA-SPK), and ECLIF III-1 (100% HEFA-SPK). The term "apparent" emphasizes that the observed ice crystals are formed indirectly through nucleation processes within the exhaust plume rather than being directly emitted by the engine [73]. Only measurements obtained under ice-supersaturated conditions ($RH_{ice} > 100\%$) were considered in the analysis.

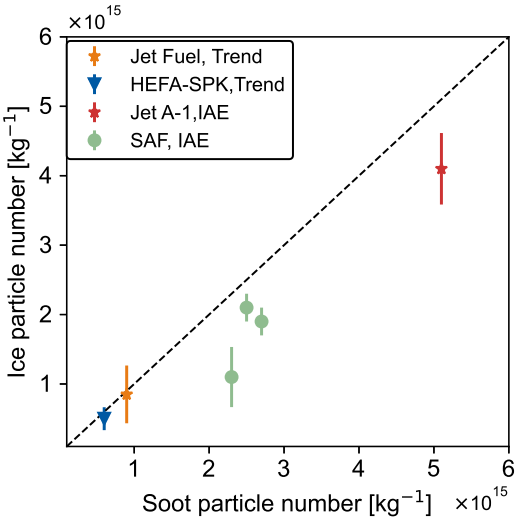

Figure 4. Correlation between N_{soot} and N_{ice}. Comparison of Jet A-1 and HEFA-SPK from the ECLIF III-1 project using a Rolls-Royce Trent XWB-84 engine, with fuels investigated during ECLIF I and ECLIF II/ND-MAX employing an IAE V2527 engine. Values adapted from [52].The cruise altitudes for the two test campaigns (35,000 ft for the Trent XWB-84 in ECLIF I and 34,000 ft for the IAEV2527 in ECLIF II/ND-MAX) are very close, yet even this $\approx$ 1000-ft difference can lead to measurable variations in soot-emission characteristics.

A pronounced quasi-linear relationship between N_{soot} and N_{ice} is evident, in agreement with the theoretical framework proposed by Kärcher [73]. The ECLIF III fuel–engine configuration exhibited substantially lower soot emissions and correspondingly reduced apparent ice crystal numbers compared with the configurations investigated during ECLIF I

and ECLIF II. This reduction is primarily attributed to the improved combustion characteristics of the Rolls-Royce Trent XWB-84 engine, which generates fewer soot particles than the older IAE V2527 engine.

The Trent XWB-84 incorporates several design advances that directly suppress soot formation. The engine has a higher overall pressure ratio (≈10:1) and a 12-stage high-pressure compressor, producing a cooler, more homogeneous mixture before combustion, lowering peak flame temperatures [89]. The Trent XWB-84 further has an advanced low-emission combustor with staged fuel injection, ultra-fine fuel atomisation and a lean-burn operating envelope. The resulting equivalence ratio is kept well below stoichiometric, which limits the soot-precursor chemistry [89]. Furthermore, the turbine-inlet temperature is optimized (≈600 °C), and a higher bypass ratio (≈9.6) reduces the exhaust gas temperature and the residence time of soot-forming radicals, further decreasing particle nucleation [89]. Finally, active cooling and a variable-area nozzle allow precise control of the exhaust plume expansion, maintaining a higher local supersaturation for ice nucleation while keeping soot concentrations low [89].

In contrast, the IAE V2527 employs a conventional annular combustor with a single-stage fuel-air mixing zone and operates at a lower overall pressure ratio (≈8:1). The higher flame temperature and less-refined mixing lead to a larger fraction of incomplete combustion, producing a higher number concentration of soot particles [90]. Consequently, the V2527-powered test flights recorded N_{soot} values up to three times those measured with the Trent XWB-84, and the associated N_{ice} followed the same quasi-linear trend but at a markedly higher magnitude.

Thus, the combination of a higher pressure ratio, lean-burn low-emission combustor technology, and improved exhaust-flow management in the Trent XWB-84 explains the observed reduction in soot emissions and the consequent decrease in apparent ice-crystal numbers in the ECLIF III campaign.

In addition, the apparent ice crystal emissions measured for Jet A-1 during ECLIF III-1 were lower than those observed for the SAF blends investigated in ECLIF I and II. These findings indicate that contrail ice formation is not solely governed by fuel composition, but is also strongly influenced by engine architecture, combustion conditions, and ambient atmospheric parameters [52]. Variations in fuel composition nevertheless play a major role in determining soot precursor formation and soot emission characteristics.

Conventional Jet A-1 contains comparatively high concentrations of aromatic compounds and PAHs, which act as important molecular precursors for soot formation and require higher oxidation energies during combustion [76]. Increasing the hydrogen content in the fuel reduces the aromatic and naphthalene fractions, thereby lowering the fuel's sooting tendency. Consequently, pure HEFA-SPK exhibited the lowest apparent N_{ice} values among the investigated fuels [52]. Furthermore, the Jet A-1 fuel used during ECLIF III, characterized by comparatively low sulfur, aromatic, and naphthalene contents, also produced lower apparent ice crystal numbers than the reference fuels employed in ECLIF I and II.

The comparison between conventional Jet A-1 and SAF blends further demonstrates that fuel composition alone cannot fully explain the observed variations in soot and ice crystal emissions. Although Jet A-1 generally contains higher aromatic fractions, lower apparent ice crystal numbers were still observed under some operating conditions. This suggests that engine-specific combustion processes, plume dilution, and ambient meteorological conditions significantly modulate soot activation and subsequent ice nucleation processes [52].

Measurements conducted during ACCESS II indicated that between 10% and 100% of emitted soot particles acted as active INPs [21], whereas ECLIF III observations suggested soot activation efficiencies of approximately 80–100%. Reduced sulfur concentrations in

SAF may suppress soot activation by limiting the formation of hydrophilic surface coatings, thereby leading to a disproportionately strong reduction in apparent ice crystal number relative to soot particle reductions alone [52]. These observations are consistent with previous findings indicating that sulfur-containing compounds enhance the hygroscopicity and hydrophilicity of soot particles, thereby facilitating heterogeneous ice nucleation [22]. In addition to fuel and engine effects, ambient atmospheric conditions exert a strong influence on contrail ice formation. In particular, correlations between N_{soot} and N_{ice} are most pronounced under conditions of low temperature and high ice supersaturation, whereas weaker supersaturation and warmer conditions can lead to substantial deviations from the quasi-linear behavior [85].

3.6. Conclusions on the Initial Ice Crystal Numbers in Contrails

The number of emitted soot particles per kilogram of burned fuel N_{soot}, their activation efficiency as INP, and the resulting apparent ice crystal number N_{ice} are governed by a complex interaction of atmospheric, technical, and experimental factors. Atmospheric conditions, particularly ambient temperature and relative humidity with respect to ice, strongly influence ice nucleation and contrail persistence. In addition, engine-related parameters such as thrust setting, combustor design, engine type, fuel composition, and blending ratio significantly affect soot formation and subsequent ice crystal production. Experimental uncertainties associated with measurement campaigns, including plume age, sampling position, test-rig configuration, and instrumental limitations, further contribute to the variability of reported particle concentrations. Methodological uncertainties must therefore also be considered when interpreting measured values.

Given these interacting factors, considerable uncertainty remains regarding the fraction of emitted soot particles that ultimately become activated as INP. Based on previously reported soot particle concentrations, a conservative upper-bound scenario is considered in which all emitted soot particles act as INP, yielding a maximum concentration of $N_{INP} = 10^{15}$ kg^{-1} fuel. Under these conditions, the apparent ice crystal number is likewise limited to approximately $N_{ice} = 10^{15}$ kg^{-1} fuel for hydrogen combustion. Consequently, the commonly stated hypothesis that SAF combustion inherently produces substantially fewer soot particles and contrail ice crystals than conventional kerosene combustion cannot be regarded as universally valid, since the resulting particle and ice crystal numbers remain strongly dependent on engine technology, operating conditions, and atmospheric conditions.

Conversely, previous numerical simulations and observational studies indicate substantially lower lower-bound estimates for contrail ice crystal formation. Based on published estimates of N_{INP} per meter of flight distance, a minimum apparent ice crystal number of $N_{ice} = 10^{9}$ kg^{-1} burned fuel is assumed for the subsequent analysis. This range between lower- and upper-bound estimates highlights the large uncertainty associated with predicting initial contrail microphysical properties, particularly for emerging propulsion concepts such as hydrogen combustion and fuel cell-powered aircraft.

4. Impact of the Initial Number of Ice Crystals on Contrail Lifetime

To assess the influence of reduced initial ice crystal number concentrations resulting from SAF and hydrogen combustion on contrail persistence and optical properties, the open-source contrail life-cycle model introduced by [91] is applied. The source code is publicly available under the Apache-2.0 license at https://github.com/jro-github/intersected_contrails/tree/main (accessed on 17 July 2026). The modeling framework has been validated under realistic atmospheric conditions through the combination of observational data, meteorological reanalysis, and aircraft performance parameters.

The model explicitly accounts for the ambient ice supersaturation ratio (rH_{ice}) and the vertical wind velocity (v_z), which represent the dominant atmospheric parameters controlling contrail persistence. Low values of rH_{ice} or pronounced downward motion generally accelerate contrail dissipation, whereas weak vertical motion combined with sustained ice supersaturation favors persistent contrails. The vertical displacement of the contrail layer is described as the balance between atmospheric vertical motion and the sedimentation velocity of the ice particles (v_{sed}), which depends primarily on the particle radius r_p.

The initial contrail geometry at the end of the vortex dissipation phase is estimated using a probabilistic wake vortex model. The duration of the dissipation regime is governed mainly by atmospheric turbulence and vortex circulation strength, both of which depend on aircraft mass, true airspeed, and wingspan. For an Airbus A320, the vortex descent phase typically lasts between 40 and 58 s, depending on atmospheric turbulence intensity. Turbulence is parameterized by the eddy dissipation rate ε [$\mathrm{m^2\,s^{-3}}$], representing the conversion of kinetic into thermal energy by viscous dissipation. A lognormal distribution of ε in the upper troposphere and lower stratosphere is assumed, with ε linearly correlated to the vertical velocity field derived from Global Forecast System (GFS) diagnostics [92].

At the onset of the dissipation regime, approximately 70–100 s after contrail formation, the wake vortices descend with a characteristic sinking velocity v_s for a duration t. Under quasi-equilibrium conditions, where lift balances aircraft weight, the descent time depends on the ambient atmospheric stratification. The initial vertical extent of the contrail is determined by the vortex radius, which scales with the tangential vortex velocity and thereby controls the ability of ice particles to remain trapped within the vortex circulation.

Following vortex decay, the contrail enters the diffusion regime, during which its evolution is governed exclusively by turbulent mixing and microphysical processes. Contrail dissipation occurs once the surrounding atmosphere becomes subsaturated with respect to ice ($rH_{\mathrm{ice}} < 100\%$) or when the ice water content falls below radiatively relevant thresholds ($IWC < 10^{-18}$ $\mathrm{kg\,m^{-3}}$). The diffusion regime is represented using a Gaussian plume formulation, in which the contrail evolves as a diffusing ice cloud with an expanding contrail cross section (CCS) and a radially decreasing Ice Water Content (IWC). The contrail geometry is approximated by a two-dimensional Gaussian distribution, where the standard deviations describe the characteristic horizontal and vertical extents. A standard atmospheric profile containing an ice-supersaturated layer between 10,000 and 11,000 m altitude is assumed, while the contrail is initialized at 10 500 m altitude. A detailed description of the methodology is provided in [93].

The evolution of the simulated contrails for varying initial ice crystal number concentrations N_{ice} is shown in Figures 5 and 6. In agreement with the conclusions drawn in the previous subsection, the initial ice crystal number concentration strongly governs the subsequent contrail microphysics and persistence. The ice crystal radius r_p represents a key parameter controlling contrail evolution. Since the simulations begin at the onset of the dissipation phase, the ice crystals already possess a finite initial radius, which subsequently increases due to depositional growth from ambient water vapor.

At low ice crystal number concentrations, the available water vapor per particle is comparatively high, resulting in rapid crystal growth and a corresponding decrease in ambient ice supersaturation. This behavior is reflected in the rapid evolution of the IWC shown in Figure 5. In contrast, high values of N_{ice} lead to enhanced competition for available water vapor, thereby limiting individual particle growth and maintaining smaller crystal radii over longer timescales. As the contrail expands and the CCS increases, additional ambient moisture becomes entrained into the plume, temporarily enhancing depositional growth until sedimentation dominates due to increasing particle mass.

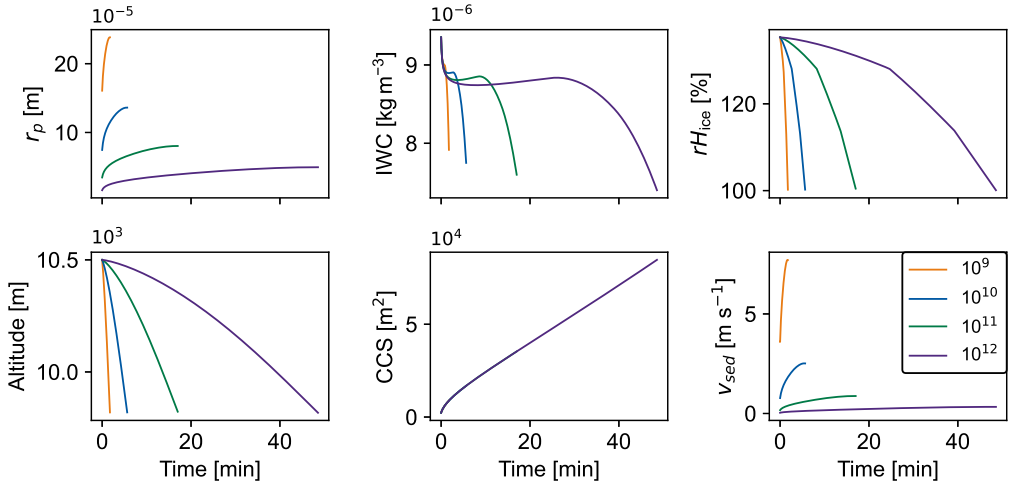

Figure 5. Ice crystal radius r_p, ice water content IWC, ice supersaturation rH_{ice}, contrail altitude, contrail cross section CCS, and sedimentation velocity v_{sed} over the lifetime of the contrails for N_{ice} between 10^9 and 10^{12} per kg of fuel burned. For H_2 combustion, $N_{\mathrm{ice}} = 10^9$–$10^{10}\,\mathrm{kg}^{-1}$ (aerosol-based) yields large ice particles and short-lived contrails, while $N_{\mathrm{ice}} \approx 10^{14}\,\mathrm{kg}^{-1}$ (homogeneous) produces persistent but less dense contrails.

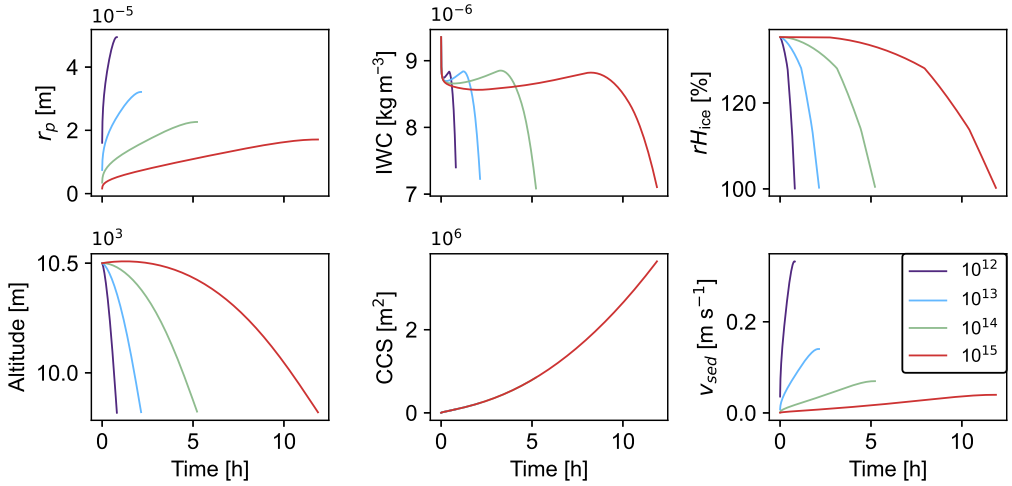

Figure 6. Evolution of ice crystal radius r_p, ice water content IWC, ice supersaturation rH_{ice}, contrail Altitude, contrail cross section CCS, and sedimentation velocity v_{sed} throughout the contrail lifetime for ice particle number concentrations N_{ice} ranging from 10^{12} to 10^{15} per kilogram of fuel burned. $N_{\mathrm{ice}} = 10^{15}$ corresponds to typical soot emission indices from burning Jet-A1 fuel. For SAF combustion, $N_{\mathrm{soot}} = N_{\mathrm{ice}} = 10^{14}$–$10^{15}\,\mathrm{kg}^{-1}$ fuel, yielding persistent contrails (9–12 h).

The sedimentation velocity v_{sed} increases with particle size, causing contrails with low N_{ice} to descend more rapidly and leave the ice-supersaturated layer sooner. Consequently, such contrails exhibit significantly shorter lifetimes. Conversely, contrails with high N_{ice} consist of smaller ice crystals with lower sedimentation velocities, allowing them to remain longer within supersaturated regions and thereby increasing their persistence. Contrail lifetime is ultimately limited either by the loss of ice supersaturation ($rH_{\mathrm{ice}} < 100\%$) or by a reduction in the ice water content below radiatively relevant values.

The simulations demonstrate that contrails characterized by low initial ice crystal number concentrations evolve rapidly and dissipate quickly due to strong sedimentation losses, whereas contrails with high N_{ice} evolve more slowly but persist for substantially longer periods. These results confirm that the initial ice crystal number concentration fundamentally controls contrail microphysical evolution, sedimentation dynamics, and persistence.

For SAF combustion, experimentally observed soot number concentrations range between 10^{14} and 10^{15} kg^{-1} fuel burned and are assumed to approximately correspond to the initial ice crystal number concentration ($N_{soot} \approx N_{ice}$). Under these conditions, the simulations yield persistent contrails with lifetimes of approximately 9–12 h.

For hydrogen-powered propulsion systems, the resulting contrail properties strongly depend on the dominant ice nucleation mechanism. If ice crystals form primarily on entrained atmospheric background aerosols, the resulting ice crystal number concentration remains comparatively low ($N_{ice} \approx 10^{9}$–10^{10} kg^{-1} fuel). Such contrails contain fewer but larger ice particles, leading to enhanced sedimentation and comparatively short-lived, often non-persistent contrails. In contrast, homogeneous nucleation driven by the high water vapor emissions from hydrogen combustion may produce substantially larger ice crystal number concentrations ($N_{ice} \approx 10^{14}$ kg^{-1} fuel). Under such conditions, persistent contrails may form. However, their ice crystal number concentrations and consequently, their optical densities are still generally lower than those associated with conventional kerosene combustion ($N_{ice} \approx 10^{15}$ kg^{-1} fuel).

Overall, the simulations indicate that the initial ice crystal number concentration represents the key parameter governing contrail persistence and microphysical evolution. Reduced initial ice crystal numbers, as expected, particularly for hydrogen propulsion systems under aerosol-limited nucleation conditions, lead to larger ice crystals, enhanced sedimentation, and substantially shorter contrail lifetimes compared to conventional kerosene-based propulsion systems.

5. Summary, Conclusions and Outlook

This study was conducted to systematically assess the potential of current alternative propulsion systems and fuels, specifically SAF and hydrogen-based technologies, for mitigating aviation-induced contrail formation and persistence, with a clear focus on identifying the key emission characteristics that govern contrail microphysics and lifetime. The primary purpose was to move beyond broad fuel comparisons and instead link measurable emission properties, such as soot particle number, water vapor, and ice-nucleating particle abundance, to the actual contrail-forming potential under realistic atmospheric conditions. By doing so, this work aims to provide a science-based framework for evaluating future propulsion technologies not only in terms of CO_2 reduction, but also in terms of their non-CO_2 climate impacts.

SAF were categorized into bio-based and synthetic pathways, while hydrogen propulsion concepts were differentiated into direct combustion and fuel cell-based systems. These technologies were compared across multiple dimensions, including technological readiness, payload capability, operational range, and preferred cruise altitude regimes, to contextualize their practical feasibility and environmental trade-offs.

The analysis demonstrated that SAF combustion produces chemical species comparable to those from conventional kerosene, although emission indices vary due to differences in fuel composition, particularly aromatic and sulfur content. Notably, soot particle emissions from currently available SAF blends often remain within the same order of magnitude as those from conventional jet fuel. This suggests that, despite the potential for reduced aromatic content, the mitigation of persistent contrail formation through SAF alone is limited, especially under atmospheric conditions where background aerosols can act as alternative INPs, partially compensating for any reductions in soot emissions.

In contrast, hydrogen propulsion systems exhibit fundamentally different emission profiles. Direct hydrogen combustion emits water vapor primarily, along with potential NO_x, metallic species, and ultrafine particles, while fuel cell-based systems emit almost exclusively water vapor. The resulting contrail properties are therefore highly sensitive to the

dominant ice nucleation mechanism. Under conditions favoring heterogeneous nucleation on ambient aerosols, ice crystal number concentrations (N_{ice}) remain low ($\approx 10^9$–10^{10} kg^{-1}), leading to larger ice crystals, faster sedimentation, and short-lived contrails (minutes). However, under conditions conducive to homogeneous nucleation, driven by high water vapor emissions, N_{ice} can increase significantly ($\approx 10^{14}$ kg^{-1}), enabling persistent contrail formation, albeit with reduced optical density and shorter lifetimes compared to kerosene-based contrails due to distinct particle growth dynamics.

The literature review further revealed that many current SAF production pathways remain partially reliant on fossil feedstocks, and their soot emission characteristics are not consistently lower than those of conventional kerosene. This underscores that the climate benefits of SAF are not guaranteed and depend critically on fuel formulation, combustion efficiency, and atmospheric context.

Overall, the results confirm that contrail formation and persistence are governed by a complex interplay between initial ice crystal number concentration (N_{ice}), ambient humidity, temperature, and the physico-chemical properties of emitted particles. Lower N_{ice} promotes rapid crystal growth and sedimentation, leading to short-lived contrails, while high N_{ice} suppresses growth and prolongs persistence. However, substantial uncertainties remain regarding the activation efficiency of soot particles as INPs, the role of ultrafine particles in hydrogen combustion, and the accurate representation of these processes in current contrail models.

In conclusion, this study emphasizes that the true climate impact of alternative propulsion systems cannot be assessed solely by fuel composition or CO_2 emissions. Instead, a comprehensive evaluation must include the microphysical evolution of contrails, driven by emission characteristics and atmospheric conditions. The findings highlight the need for future research to focus on in-flight measurements of INP emissions, improved characterization of soot and ultrafine particle properties, and the development of more accurate contrail models that account for nucleation mechanisms and particle growth dynamics. Only by integrating these elements can we reliably assess the actual contrail mitigation potential of emerging aviation technologies and support informed decision-making toward truly climate-neutral aviation.

Future research should therefore focus on improving both the experimental and numerical basis for contrail prediction. In particular, dedicated in-flight and ground-based measurements under representative cruise conditions are required to quantify the emissions, aerosol characteristics, and ice-nucleating properties of hydrogen combustion products and fuel cell exhaust. Furthermore, the physicochemical properties of atmospheric aerosol particles that determine their effectiveness as INP should be investigated in greater detail. Existing contrail life-cycle and microphysical models should additionally be refined through the incorporation of realistic particle size distributions, stochastic atmospheric variability, aerosol–cloud interactions, and improved representations of optical properties.

In parallel, continued optimization of SAF composition remains essential for mitigating aviation-induced non-CO_2 climate effects. Reductions in aromatic and sulfur content, combined with increased hydrogen-to-carbon ratios, may further decrease soot formation and reduce contrail ice crystal concentrations. Together with advances in lean-burn combustor technologies and low-emission propulsion concepts, these developments may contribute significantly to lowering the climatic impact of aviation beyond direct CO_2 emissions.

Author Contributions: Conceptualization, J.R.; methodology, J.R.; software, J.R.; validation, J.R.; formal analysis, J.R.; investigation, J.R.; resources, T.F.G. and L.E.; data curation J.R.; writing—original draft preparation, J.R.; writing—review and editing, J.R.; visualization, J.R.; supervision, J.R.; project administration, J.R.; funding acquisition, T.F.G. and L.E. All authors have read and agreed to the published version of the manuscript.

Funding: This research received no external funding.

Data Availability Statement: In this study, the open-source contrail life-cycle model introduced by [91] is applied. The source code is publicly available under the Apache-2.0 license at https://github.com/jro-github/intersected_contrails (accessed on 17 July 2026).

Acknowledgments: This work contributes to the research initiative ICATO (Individual Condensation Trails in Aircraft Trajectory Optimization), which serves as the overarching framework for the author's research on contrail mitigation. (https://github.com/jro-github/icato.github.io) (accessed on 12 August 2026).

Conflicts of Interest: The authors declare no conflicts of interest.

References

1. Schumann, U. On conditions for Contrail formation from aircraft exhaust. *Meteorol. Z.* **1996**, *5*, 4–23.
2. Lee, D.; Fahey, D.; Skowron, A.; Allen, M.; Burkhardt, U.; Chen, Q.; Doherty, S.; Freeman, S.; Forster, P.; Fuglestvedt, J.; et al. The contribution of global aviation to anthropogenic climate forcing for 2000 to 2018. *Atmos. Environ.* **2021**, *244*, 117834. [CrossRef] [PubMed]
3. Kärcher, B.; Kleine, J.; Sauer, D.; Voigt, C. Contrail Formation: Analysis of Sublimation Mechanisms. *Geophys. Res. Lett.* **2018**, *45*, 13547–13552. [CrossRef]
4. Intergovernmental Panel on Climate Change (IPCC). *Climate Change 2023: Synthesis Report*; Sixth Assessment Report (AR6), Synthesis Report; United Nations (UN) Intergovernmental Panel on Climate Change (IPCC): Geneva, Switzerland, 2023.
5. Schumann, U.; Heymsfield, A. On the lifecycle of individual contrails and contrail cirrus. *AMS Meteorol. Monogr.* **2017**, *58*, 3.1–3.24. [CrossRef]
6. Teoh, R.; Engberg, Z.; Schumann, U.; Voigt, C.; Shapiro, M.; Rohs, S.; Stettler, M.E.J. Global aviation contrail climate effects from 2019 to 2021. *Atmos. Chem. Phys.* **2024**, *24*, 6071–6093. [CrossRef]
7. Prather, M.; Gettelman, A.; Penner, J. Trade-offs in aviation impacts on climate favour non-CO_2 mitigation. *Nature* **2025**, *643*, 988–993. [CrossRef] [PubMed]
8. Xu, D. Technologies and challenges of hydrogen powered aviation. *J. Phys. Conf. Ser.* **2023**, *2608*, 012003. [CrossRef]
9. Gierens, K. Theory of Contrail Formation for Fuel Cells. *Aerospace* **2021**, *8*, 164. [CrossRef]
10. Burkhardt, U.; Kärcher, B. Global radiative forcing from contrail cirrus. *Nat. Clim. Change* **2011**, *1*, 54–58. [CrossRef]
11. Hudson, J.G. Cloud Condensation Nuclei. *J. Appl. Meteorol. Climatol.* **1993**, *32*, 596–607. [CrossRef] [PubMed]
12. Kulkarni, G.; Mei, F.; Shilling, J.; Wang, J.; Reveggino, R.; Flynn, C.; Zelenyuk, A.; Fast, J. Cloud Condensation Nuclei Closure Study Using Airborne Measurements Over the Southern Great Plains. *J. Geophys. Res. Atmos.* **2023**, *128*, e2022JD037964. [CrossRef]
13. Charlson, R.J.; Lovelock, J.E.; Andreae, M.O.; Warren, S.G. Oceanic phytoplankton, atmospheric sulphur, cloud albedo and climate. *Nature* **1987**, *326*, 655–661. [CrossRef]
14. Horowitz, H.M.; Holmes, C.; Wright, A.; Sherwen, T.; Wang, X.; Evans, M.; Huang, J.; Jaeglé, L.; Chen, Q.; Zhai, S.; et al. Effects of Sea Salt Aerosol Emissions for Marine Cloud Brightening on Atmospheric Chemistry: Implications for Radiative Forcing. *Geophys. Res. Lett.* **2020**, *47*, e2019GL085838. [CrossRef] [PubMed]
15. Baker, M.B.; Charlson, R.J. Bistability of CCN concentrations and thermodynamics in the cloud-topped boundary layer. *Nature* **1990**, *345*, 142–145. [CrossRef]
16. Yu, F.; Luo, G. Effect of solar variations on particle formation and cloud condensation nuclei. *Environ. Res. Lett.* **2014**, *9*, 045004. [CrossRef]
17. Myhre, G.; Shindell, D.; Bréon, F.M.; Collins, W.; Fuglestvedt, J.; Huang, J.; Koch, D.; Lamarque, J.F.; Lee, D.; Mendoza, B.; et al. Anthropogenic and Natural Radiative Forcing. In *Climate Change 2013: The Physical Science Basis. Contribution of Working Group I to the Fifth Assessment Report of the Intergovernmental Panel on Climate Change*; Cambridge University Press: Cambridge, UK, 2013.
18. Lovelock, J. *The Revenge of Gaia: Why the Earth Is Fighting Back—And How We Can Still Save Humanity*; Penguin: London, UK, 2007.
19. Arghavani, S.; Rose, C.; Banson, S.; Planche, C.; Sellegri, K. The Effect of using a New Parameterization of Nucleation in the WRF-Chem model on the Cluster Formation Rate and Particle Number Concentration in a Passive Volcanic Plume. In *Proceedings of the EGU General Assembly Conference Abstracts*; Copernicus GmbH: Göttingen, Germany, 2021; Volume 23, p. EGU21-12058. [CrossRef]
20. Rosenow, J.; Köhler, S.; Geyer, T. Emission characteristics of alternative drive technologies regarding type and number of condensation nuclei for contrail formation. In Proceedings of the 10th CEAS Aerospace Europe Conference/28th AIDAA International Congress, Turin, Italy, 1–4 December 2025.
21. Anderson, B. *Alternative-Fuel Effects on Contrails & Cruise Emissions (ACCESS-2) Flight Experiment*; Technical Report; NASA: Washington, DC, USA, 2016.

22. Jones, S.H.; Miake-Lye, R.C. Contrail Modeling of ECLIF2/ND-MAX Flights: Effects of nvPM Particle Numbers and Fuel Sulfur Content. *Meteorol. Z.* **2024**, *33*, 35–41. [CrossRef]
23. Moore, R.H.; Thornhill, K.L.; Weinzierl, B.; Sauer, D.; D'Ascoli, E.; Kim, J.; Lichtenstern, M.; Scheibe, M.; Beaton, B.; Beyersdorf, A.J.; et al. Biofuel blending reduces particle emissions from aircraft engines at cruise conditions. *Nature* **2017**, 543, 411–415. [CrossRef] [PubMed]
24. Voigt, C.; Kleine, J.; Sauer, D.; Moore, R.H.; Bräuer, T.; Le Clercq, P.; Kaufmann, S.; Scheibe, M.; Jurkat-Witschas, T.; Aigner, M.; et al. Cleaner burning aviation fuels can reduce contrail cloudiness. *Commun. Earth Environ.* **2021**, *2*, 114. [CrossRef]
25. Nobili, A.; Veltri, M.; D'Andria, M.; Pelucchi, M.; Faravelli, T.; Mehl, M. A kinetic study on the blending behavior of sustainable and conventional aviation fuels: Soot formation processes. *Proc. Combust. Inst.* **2024**, *40*, 105761. [CrossRef]
26. Hafis, M.; Balaji, K.; Tamilarasan, N.; Senthilkumar, D.; Sakthivel, R. A review on alternative fuels: Spray characteristics, engine performance and emissions effect. *Sustain. Futur.* **2025**, *9*, 100456. [CrossRef]
27. Verstraete, D. Long range transport aircraft using hydrogen fuel. *Int. J. Hydrogen Energy* **2013**, *38*, 14824–14831. [CrossRef]
28. Brewer, G. *Hydrogen Aircraft Technology*; CRC Press: New York, NY, USA, 2017; pp. 1–432. [CrossRef]
29. Yusaf, T.; Fernandes, L.; Abu Talib, A.R.; Altarazi, Y.S.M.; Alrefae, W.; Kadirgama, K.; Ramasamy, D.; Jayasuriya, A.; Brown, G.; Mamat, R.; et al. Sustainable Aviation—Hydrogen Is the Future. *Sustainability* **2022**, *14*, 548. [CrossRef]
30. Voigt, C.; Märkl, R.; Sauer, D.; Dischl, R.; Renard, C.; Seeliger, K.; Yu, F.; Kaufmann, S.; Bräuer, T.; Jurkat, T.; et al. Substantial aircraft contrail formation at low soot emission levels. *Nature* **2026**, *652*, 112–118. [CrossRef] [PubMed]
31. International Civil Aviation Organization. *Annex 16 to the Convention on International Civil Aviation– Environmental Protection*, 2nd ed.; ICAO: Montreal, QC, Canada, 2023; Volume IV, 124p.
32. European Parliament and Council of the European Union. Directive (EU) 2018/2001 of the European Parliament and of the Council of 11 December 2018 on the Promotion of the Use of Energy from Renewable Sources (Recast). *Off. J. Eur. Union* **2018**, *L 328*, 82–209.
33. Kadam, P.; Dwivedi, P. Inflight Sustainability: Harmonizing Certification Standards for Sustainable Aviation Fuel Adoption. *BioEnergy Res.* **2026**, *19*, 11. [CrossRef]
34. *ASTM D7566-24*; Standard Specification for Aviation Turbine Fuel Containing Synthesized Hydrocarbons. Current Specification for Synthetic Aviation Turbine Fuels. ASTM International: Conshohocken, PA, USA, 2024.
35. *ASTM D1655-24b*; Standard Specification for Aviation Turbine Fuels. ASTM International: Conshohocken, PA, USA, 2024.
36. Pavlenko, N.; Searle, S.; Christensen, A. *The Cost of Supporting Alternative Jet Fuels in the European Union*; Discussion of Sustainability and Co-Processing Concerns; International Council on Clean Transportation (ICCT): Washington, DC, USA, 2019.
37. Prussi, M.; O'Connell, A.; Lonza, L. Analysis of current aviation biofuel technical production potential in EU28. *Biomass Bioenergy* **2019**, *130*, 105371. [CrossRef]
38. Staples, M.D.; Malina, R.; Barrett, S.R. The Limits of Bioenergy for Mitigating Global Life-Cycle Greenhouse Gas Emissions from Fossil Fuels. *Nat. Energy* **2017**, *2*, 16202. [CrossRef]
39. Rojas-Michaga, M.F.; Michailos, S.; Cardozo, E.; Akram, M.; Hughes, K.J.; Ingham, D.; Pourkashanian, M. Sustainable aviation fuel (SAF) production through power-to-liquid (PtL): A combined techno-economic and life cycle assessment. *Energy Convers. Manag.* **2023**, *292*, 117427. [CrossRef]
40. Klimczyk, W.; Jasiński, R.; Niklas, J.; Siedlecki, M.; Ziółkowski, A. Sustainable Aviation Fuels: A Comprehensive Review of Production Pathways, Environmental Impacts, Lifecycle Assessment, and Certification Frameworks. *Energies* **2025**, *18*, 3705. [CrossRef]
41. Brynolf, S.; Taljegard, M.; Grahn, M.; Hansson, J. Electrofuels for the transport sector: A review of production costs. *Renew. Sustain. Energy Rev.* **2018**, *81*, 1887–1905. [CrossRef]
42. Ail, S.S.; Dasappa, S. Biomass to liquid transportation fuel via Fischer Tropsch synthesis - Technology review and current scenario. *Renew. Sustain. Energy Rev.* **2016**, *58*, 267–286. [CrossRef]
43. Akhtar, M.U.S.; Asfand, F.; Mishamandani, A.S.; Mishra, R.; Khan, M.I. Hydrogen as a sustainable combustion fuel: Performance, challenges, and pathways for transition to low-carbon propulsion systems. *Renew. Sustain. Energy Rev.* **2025**, *223*, 116004. [CrossRef]
44. Franke, F.; Kazula, S. Conceptual Design of a Metal Hydride System for the Recovery of Gaseous Hydrogen Boil-off Losses from LH2 Tanks. *Aeronaut. J.* **2025**, *130*, 1–15. [CrossRef]
45. Rempe, S.; Mischke, M.; Lachmund, M.; Geyer, T.F. Analysis of Specific Failure Conditions in Electrified Propulsion Systems Using Cryogenic Hydrogen as a Primary Energy Carrier. *CEAS Aeronaut. J.* **2026**, *17*, 841–854. [CrossRef]
46. Kazula, S.; de Graaf, S.; Enghardt, L. Review of fuel cell technologies and evaluation of their potential and challenges for electrified propulsion systems in commercial aviation. *J. Glob. Power Propuls. Soc.* **2023**, *7*, 43–57. [CrossRef]
47. International Civil Aviation Organization (ICAO). *Consolidated Statement of Continuing ICAO Policies and Practices Related to Environmental Protection–Climate Change. Presented at the 37th Session of the ICAO Assembly*; Technical Report A37-WP/25; ICAO: Montreal, QC, Canada, 2010.

48. Wang, M.; Yu, X. An Overview of the Sustainable Aviation Fuel: LCA, TEA, and the Sustainability Analysis. *Eng. Proc.* **2024**, *80*, 3. [CrossRef]
49. Hoff, T.; Becker, F.; Dadashi, A.; Wicke, K.; Wende, G. Implementation of Fuel Cells in Aviation from a Maintenance, Repair and Overhaul Perspective. *Aerospace* **2023**, *10*, 23. [CrossRef]
50. Braun-Unkhoff, M.; Riedel, U.; Wahl, C. About the Emissions of Alternative Jet Fuels. *CEAS Aeronaut. J.* **2017**, *8*, 167–180. [CrossRef]
51. Lee, D.S.; Fahey, D.W.; Forster, P.M.; Newton, P.J.; Witt, R.C.; Lim, L.L.; Owen, B.; Sausen, R. Aviation and global climate change in the 21st century. *Atmos. Environ.* **2009**, *43*, 3520–3537. [CrossRef] [PubMed]
52. Märkl, R.S.; Voigt, C.; Sauer, D.; Dischl, R.K.; Kaufmann, S.; Harlaß, T.; Hahn, V.; Roiger, A.; Weiß-Rehm, C.; Burkhardt, U.; et al. Powering aircraft with 100% sustainable aviation fuel reduces ice crystals in contrails. *Atmos. Chem. Phys.* **2024**, *24*, 3813–3837. [CrossRef]
53. Moore, R.H.; Shook, M.; Beyersdorf, A.; Beyersdorf, A.; Anderson, B.E. Influence of Jet Fuel Composition on Aircraft Engine Emissions: A Synthesis of Aerosol Emissions Data from the NASA APEX, AAFEX, and ACCESS Missions. *Energy Fuels* **2015**, *29*, 2591–2600. [CrossRef]
54. Bahr, D.W. Gas Turbine Combustion—Alternative Fuels and Emission. *J. Eng. Gas Turbines Power* **2010**, *132*, 116501. [CrossRef]
55. Przysowa, R.; Gawron, B.; Bialecki, T.; Legowik, A.; Merkisz, J.; Jasinski, R. Performance and Emissions of a Microturbine and Turbofan Powered by Alternative Fuels. *Aerospace* **2021**, *8*, 25. [CrossRef]
56. Gawron, B.; Białecki, T.; Janicka, A.; Suchocki, T. Combustion and Emissions Characteristics of the Turbine Engine Fueled with HEFA Blends from Different Feedstocks. *Energies* **2020**, *13*, 1277. [CrossRef]
57. Song, Z.; Li, Z.; Liu, Z. Comparison of Emission Properties of Sustainable Aviation Fuels and Conventional Aviation Fuels: A Review. *Appl. Sci.* **2024**, *14*, 5484. [CrossRef]
58. Lobo, P.; Hagen, D.E.; Whitefield, P.D. Comparison of PM Emissions from a Commercial Jet Engine Burning Conventional, Biomass, and Fischer–Tropsch Fuels. *Environ. Sci. Technol.* **2011**, *45*, 10744–10749. [CrossRef] [PubMed]
59. Tran, S.; Brown, A.; Olfert, J.S. Comparison of Particle Number Emissions from In-Flight Aircraft Fueled with Jet A1, JP-5 and an Alcohol-to-Jet Fuel Blend. *Energy Fuels* **2020**, *34*, 7218–7222. [CrossRef]
60. Chan, T.W.; Chishty, W.A.; Canteenwalla, P.; Buote, D.; Davison, C.R. Characterization of Emissions from the Use of Alternative Aviation Fuels. *J. Eng. Gas Turbines Power* **2015**, *138*, 011506. [CrossRef]
61. Zeldovich, Y.B. The Oxidation of Nitrogen in Combustion Explosions. *J. Acta Physicochim.* **1946**, *21*, 577–628.
62. Booz Allen Hamilton and Environmental Consulting Group and Missouri University of Science and Technology and Csonka Aviation Consultancy, LLC. *State of the Industry Report on Air Quality Emissions from Sustainable Alternative Jet Fuels*; The National Academies Press: Washington, DC, USA, 2018. [CrossRef] [PubMed]
63. Richter, H.; Howard, J.B. Formation of polycyclic aromatic hydrocarbons and their growth to soot—A review of chemical reaction pathways. *Prog. Energy Combust. Sci.* **2000**, *26*, 565–608. [CrossRef]
64. Lefebvre, A.; Ballal, D. *Gas Turbine Combustion: Alternative Fuels and Emissions*, 3rd ed.; CRC Press: Boca Raton, FL, USA, 2010. [CrossRef]
65. Khan, M.A.H.; Brierley, J.; Tait, K.N.; Bullock, S.; Shallcross, D.E.; Lowenberg, M.H. The Emissions of Water Vapour and NOx from Modelled Hydrogen-Fuelled Aircraft and the Impact of NOx Reduction on Climate Compared with Kerosene-Fuelled Aircraft. *Atmosphere* **2022**, *13*, 1660. [CrossRef]
66. Ungeheuer, F.; Caudillo, L.; Ditas, F.; Simon, M.; van Pinxteren, D.; Kılıç, D.; Rose, D.; Jacobi, S.; Kürten, A.; Curtius, J.; et al. Nucleation of jet engine oil vapours is a large source of aviation-related ultrafine particles. *Commun. Earth Environ.* **2022**, *3*, 319. [CrossRef]
67. Bier, A.; Unterstrasser, S.; Zink, J.; Hillenbrand, D.; Jurkat-Witschas, T.; Lottermoser, A. Contrail formation on ambient aerosol particles for aircraft with hydrogen combustion: A box model trajectory study. *Atmos. Chem. Phys.* **2024**, *24*, 2319–2344. [CrossRef]
68. Wiegand, M.; Schuchard, L.; Lauro, S.; Lange, M.; Mailach, R. Fuel Cell Hybrid-Electric Aircraft Performance: Optimizing Thermal Management for Reduced Climate Impact. In *Proceedings of the ASME Turbo Expo 2025: Turbomachinery Technical Conference and Exposition, Memphis, TN, USA*; ASME: New York, NY, USA, 2025. [CrossRef]
69. Cavini, L.; Liscouët-Hanke, S.; Viola, N. A causal Fuel Cell Simulation Model for System Integration Analysis in Early Design Phases. *Modelling* **2024**, *5*, 1435–1453. [CrossRef]
70. Rosenow, J.; Geyer, T.F. Impact of Fuel-Cell Stack Size and Atmospheric Conditions on Contrail Formation. In *Proceedings of the New Trends in Civil Aviation (NTCA), Prague, Czech Republic 2026*; IEEE: Piscataway, NJ, USA, 2026.
71. Schneider, J.; Höhler, K.; Wagner, R.; Saathoff, H.; Schnaiter, F.M.; Schorr, T.; Steinke, I.; Benz, S.; Baumgartner, M.; Rolf, C.; et al. High homogeneous freezing onsets of sulfuric acid aerosol at cirrus temperatures. *Atmos. Chem. Phys.* **2021**, *21*, 14403–14425. [CrossRef]
72. Kanji, Z.A.; Ladino, L.A.; Wex, H.; Boose, Y.; Burkert-Kohn, M.; Cziczo, D.J.; Krämer, M. Overview of Ice Nucleating Particles. *Meteorol. Monogr.* **2017**, *58*, 1.1–1.33. [CrossRef]

73. K"archer, B.; Yu, F. Role of aircraft soot emissions in contrail formation. *Geophys. Res. Lett.* **2009**, *36*, 1. [CrossRef]
74. Cziczo, D.J.; Stetzer, O.; Worringen, A. Inadvertent climate modification due to anthropogenic lead. *Nat. Geosci.* **2009**, *2*, 333–336. [CrossRef]
75. Kleine, J.; Voigt, C.; Sauer, D.; Schlager, H.; Scheibe, M.; Jurkat-Witschas, T.; Kaufmann, S.; Kärcher, B.; Anderson, B.E. In Situ Observations of Ice Particle Losses in a Young Persistent Contrail. *Geophys. Res. Lett.* **2018**, *45*, 13553–13561. [CrossRef]
76. Dischl, R.; Sauer, D.; Voigt, C.; Harlaß, T.; Sakellariou, F.; Märkl, R.; Schumann, U.; Scheibe, M.; Kaufmann, S.; Roiger, A.; et al. Measurements of particle emissions of an A350-941 burning 100% sustainable aviation fuels in cruise. *Atmos. Chem. Phys.* **2024**, *24*, 11255–11273. [CrossRef]
77. Harlass, T.; Dischl, R.; Kaufmann, S.; Märkl, R.; Sauer, D.; Scheibe, M.; Stock, P.; Bräuer, T.; Dörnbrack, A.; Roiger, A.; et al. Measurement report: In-flight and ground-based measurements of nitrogen oxide emissions from latest-generation jet engines and 100 sustainable aviation fuel. *Atmos. Chem. Phys.* **2024**, *24*, 11807–11822. [CrossRef]
78. Schripp, T.; Anderson, B.E.; Bauder, U.; Rauch, B.; Corbin, J.C.; Smallwood, G.J.; Lobo, P.; Crosbie, E.C.; Shook, M.A.; Miake-Lye, R.C.; et al. Aircraft engine particulate matter emissions from sustainable aviation fuels: Results from ground-based measurements during the NASA/DLR campaign ECLIF2/ND-MAX. *Fuel* **2022**, *325*, 124764. [CrossRef]
79. Durdina, L.; Brem, B.T.; Elser, M.; Schönenberger, D.; Siegerist, F.; Anet, J.G. Reduction of Nonvolatile Particulate Matter Emissions of a Commercial Turbofan Engine at the Ground Level from the Use of a Sustainable Aviation Fuel Blend. *Environ. Sci. Technol.* **2021**, *55*, 14576–14585. [CrossRef] [PubMed]
80. Bräuer, T.; Voigt, C.; Sauer, D.; Kaufmann, S.; Hahn, V.; Scheibe, M.; Schlager, H.; Diskin, G.S.; Nowak, J.B.; DiGangi, J.P.; et al. Airborne Measurements of Contrail Ice Properties—Dependence on Temperature and Humidity. *Geophys. Res. Lett.* **2021**, *48*, e2020GL092166. [CrossRef]
81. Xu, Z.; Wang, M.; Chang, L.; Pan, K.; Shen, X.; Zhong, S.; Xu, J.; Liu, L.; Li, G.; Chen, L. Assessing the particulate matter emission reduction characteristics of small turbofan engines fueled with 100% HEFA sustainable aviation fuel. *Sci. Total Environ.* **2024**, *945*, 174128. [CrossRef] [PubMed]
82. NASA. Aeronautics Field Projects for NASA Aeronautics Research Mission Directorate. Available online: https://www.nasa.gov/directorates/armd/ (accessed on 14 October 2025).
83. Schripp, T.; Anderson, B.; Crosbie, E.C.; Moore, R.H.; Herrmann, F.; Oßwald, P.; Wahl, C.; Kapernaum, M.; Köhler, M.; Le Clercq, P.; et al. Impact of Alternative Jet Fuels on Engine Exhaust Composition During the 2015 ECLIF Ground-Based Measurements Campaign. *Environ. Sci. Technol.* **2018**, *52*, 4969–4978. [CrossRef] [PubMed]
84. Ström, L.; Gierens, K. First simulations of cryoplane contrails. *J. Geophys. Res. Atmos.* **2002**, *107*, AAC 2-1–AAC 2-13. [CrossRef]
85. Lottermoser, A.; Unterstrasser, S. High-resolution modelling of early contrail evolution from hydrogen-powered aircraft. *EGUsphere* **2025**, 1–33. [CrossRef]
86. Gierens, K. On the transition between heterogeneous and homogeneous freezing. *Atmos. Chem. Phys.* **2003**, *3*, 437–446. [CrossRef]
87. Beer, C.G.; Hendricks, J.; Righi, M. A global climatology of ice-nucleating particles under cirrus conditions derived from model simulations with MADE3 in EMAC. *Atmos. Chem. Phys.* **2022**, *22*, 15887–15907. [CrossRef]
88. Narciso, M.; de Sousa, J.M.M. Influence of Sustainable Aviation Fuels on the Formation of Contrails and Their Properties. *Energies* **2021**, *14*, 5557. [CrossRef]
89. Rolls-Royce plc. *Trent XWB-84: Advanced Low-Emission Combustor and High-Pressure Ratio Design*; Technical Report RR-TR-XWB-84-2020; Rolls-Royce plc: London, UK, 2020.
90. International Aero Engines (IAE). *V2527-AE Engine—Design Overview and Emission Characteristics*; Technical Report IAE-V2527-2021; International Aero Engines: East Hartford, CT, USA, 2021.
91. Rosenow, J.; Luo, M. A Contrail Life Cycle Model with Interaction of Overlapping Contrails. *Aerospace* **2026**, *13*, 164. [CrossRef]
92. Sharman, R.D.; Pearson, J.M. Prediction of Energy Dissipation Rates for Aviation Turbulence. Part I: Forecasting Nonconvective Turbulence. *J. Appl. Meteorol. Climatol.* **2017**, *56*, 317–337. [CrossRef]
93. Rosenow, J.; Köhler, S. Astronomical, Atmospheric, and Lifetime-specific Requirements for Cooling Contrails. In Proceedings of the SESAR Innovation Days 2024, Rome, Italy, 12–15 November 2024. . [CrossRef]

Disclaimer/Publisher's Note: The statements, opinions and data contained in all publications are solely those of the individual author(s) and contributor(s) and not of MDPI and/or the editor(s). MDPI and/or the editor(s) disclaim responsibility for any injury to people or property resulting from any ideas, methods, instructions or products referred to in the content.